

# A Tridomain Model for Potassium Clearance in Optic Nerve

Yi Zhu<sup>1</sup>, Shixin Xu<sup>2,\*</sup>, Robert S. Eisenberg<sup>3,4</sup>, and Huaxiong Huang<sup>5,6,1</sup>

[1] Department of Mathematics and Statistics, York University, Toronto, ON, M3J 1P3, Canada

[2] Duke Kunshan University, 8 Duke Ave., Kunshan, Jiangsu, China

[3] Department of Applied Mathematics, Illinois Institute of Technology, Chicago IL 60616 USA

[4] Department of Physiology & Biophysics, Rush University Chicago IL 60612, USA

[5] Research Centre for Mathematics, Advanced Institute of Natural Sciences, Beijing Normal University (Zhuhai), China

[6] BNU- HKBU United International College, Zhuhai, China

## ABSTRACT

The accumulation of potassium in the narrow space outside nerve cells is a classical subject of biophysics that has received much attention recently. It may be involved in potassium accumulation include spreading depression, perhaps migraine and some kinds of epilepsy, even (speculatively) learning. Quantitative analysis is likely to help evaluate the role of potassium clearance from the extracellular space after a train of action potentials. Clearance involves three structures that extend down the length of the nerve: glia, extracellular space, and axon and so need to be described in the tradition of the ‘cable equations’ of nerve used to explain nerve conduction since the work of Hodgkin in 1937. A three-compartment model is proposed here for the optic nerve and is used to study the accumulation of potassium and its clearance. The model allows the convection, diffusion, and electrical migration of water and ions. We depend on the data of Orkand et al to ensure the relevance of our model and align its parameters with the anatomy and properties of membranes, channels, and transporters: our model fits their experimental data quite well. The aligned model shows that glia has an important role in buffering potassium, as expected. The model shows that potassium is cleared mostly by convective flow through the syncytia of glia driven by osmotic pressure differences. A simplified model might be possible, but it must involve flow down the length of the optic nerve. It is easy for compartment models to neglect this flow. Our model can be used for structures quite different from the optic nerve that might have different distributions of channels and transporters in its three compartments. It can be generalized to include the fourth compartment to deal with the glymphatic flow into the circulatory system.

## 1. Introduction

The now classical experiments of Hodgkin, Huxley, and Katz [1, 2] were designed to avoid the artifact of concentration polarization, the (significant) change of concentration of ions as the currents maintaining their voltage clamp flowed across electrodes inside the axon and its membranes. Change of concentration of potassium was seen nonetheless after a few milliseconds of outward potassium currents ([3]: p. 482, 485, 489, 494); [4]), but the change was slow enough to be ignored in their calculations of the action potential [5].

The Kuffler group at Harvard was interested in the role of glia [6, 7] in the central nervous system and showed that the membrane potential of the optic nerve of *Necturus* reported the potassium concentration in the narrow extracellular space just outside axons, between glia and axon. Orkand et al [8] used this membrane potential of glia to report the change in potassium concentration—the polarization of concentration in the narrow extracellular space—as it accumulated during a train of nerve action potentials. Earlier work [3, 4] had inferred this concentration change. Orkand et al (7) measured it quite directly. The artifact of concentration polarization that so worried Hodgkin and Huxley became the experimental reality of potassium accumulation [3] in the central nervous system [8], that interested the Kuffler group. Interest has only grown in the following fifty some odd years.

Potassium accumulation and flow in the extracellular space have been shown to have important roles in many papers focused on aging, Alzheimers disease, anesthesia, dementia, diabetes, epilepsy, migraine, sleep, stroke and traumatic brain injury. Potassium accumulation and flow play an important role in the biology of the central nervous system [9] normal, and abnormal [10-17]. The glymphatic model has received much interest in the last months. It links potassium accumulation, flows in the extracellular space—particularly in sleep and diseases of aging—with general disposal of waste through glial pathways to the circulatory system [9, 18-22].

The accumulation of ions in a narrow extracellular space, like that between nerve and glia, or Schwann cell [4], depends on the diffusion, convection, and migration of ions in an electric field. Convection is likely to be important. Evolution uses the circulatory system to provide convective transport close to nearly every cell in a mammal, so the delays involved in electrodiffusion are overcome. Convection provides what diffusion denies: speed.

We have analyzed flow in systems with narrow extracellular spaces, starting with a derivation [23] of the fundamental osmotic equations [24], using a ~~variational~~ method that ensures mathematical consistency [25]: all variables must satisfy the field equations of convection, diffusion, and electrical migration and their boundary conditions, including the internal membrane ‘boundary’ conditions within the external

boundary [23], with one set of unchanging parameters.

The field equations were first applied to the lens of eye because that tissue is so dependent on an 'electroosmotic pump' to provide nutrients and remove wastes [26-30]. The lens of the eye contains no blood vessels. Its circulatory system is provided by its membranes, by flows through its ion channels and transporters. One might say the mechanical pump of the heart is replaced by an electro-osmotic pump of transporters and channels, if one is allowed some vivid words.

The lens has been studied with great success, led by the Mathias group, starting with an engineering model (Fig.1 of [31] and [32]) providing a unified understanding of how its membranes, transporters and channels act together to form its electro-osmotic pump. Measurements of electrical structure were done with high resolution impedance spectroscopy [33, 34], interpreted with a general theory of syncytial tissues [35], and then extended to measurements of pressure [36-38], and effects of many experimental interventions and manipulations [38-42] normal, and abnormal [10-13, 16, 17, 43]. Along the way, the general (i.e., epithelial) phenomenon of isotonic flow was analyzed [44, 45]. Long standing controversies in epithelial physiology were dissolved by mathematical solutions once pressure, convection, diffusion, and migration were treated in a consistent local model of osmosis replacing inconsistent models [46-50].

Our field theory approach to the lens [51] generalizes the engineering approach. It derives the engineering models, using standard methods of applied and numerical mathematics, without *ad hoc* assumptions. It provides more resolution of some key physiological parameters like internal hydrostatic pressure and gives a more complete understanding of the role of internal structures and channels. A mathematically complete, and consistent treatment is more likely to lead to specific understanding of biological function than models that are less well related to fundamental physical laws. In particular, models are hard to pin down that use computer programs with many equations and difficult (or impossible) to measure parameters to describe structural details of the system [52-58]. Such models are not easy to check [59-61], both for unavoidable programming errors [62], or for consistency with fundamental laws of diffusion, convection, and electrical migration, including conservation of mass, charge and current.

Here we extend the two-compartment structural analysis of the spherical lens to the three-compartment cylindrical optic nerve fiber of ***Necturus***. We generalized our lens theory from two to three compartments and derived, computed, and report the results appropriate for a cylindrical geometry.

The optic nerve, and the mammalian central nervous system in general, involves nerve, glia and narrow extracellular space. It involves three types of flow, convection, diffusion, and migration in the electric field in radial and longitudinal directions of a

cylindrical structure. It involves (chiefly) three ions (K, Na, Cl), and a number of different types of channels and pumps (voltage activated Na channels and at least two types of K channels and the Na/K pump). The description and analysis, not to say the numerical computation of the optic nerve, must deal with what is actually in the optic nerve. It must deal with what evolution has actually built in the central nervous system in general. Thus, the analysis must involve many forces, flows, structures, and channels and transporters. Here we report the subset of our work that deals with the accumulation of potassium in the narrow extracellular space of optic nerve.

The importance of the experimental results of Orkand et al [8] cannot be overstated both for our tridomain model, and for our general approach to constructing useful models of biological systems. Without measurements of structure and function, probing a range of conditions, it is all to easy to be lost in the large space of possible parameters in a structure as complex as the optic nerve, as it would have been in the lens of the eye, without the experimental work, led by Mathias group [30]. The available results provide a most important target for our analysis, ensuring that our theory and its parameters describe real structures so they can deal with experimental reality in an actual central nervous system.

This paper is organized as follows. The full model for microcirculation of water and ions are proposed based on conservation laws in Mathematical Model. Then the model is calibrated with the Orkand experiment results in Model Calibration. The calibrated model is used to study the flow and ion microcirculations during Potassium clearance. The conclusions and future work are given in Conclusions.

## 2. Mathematical Model

In this section, we present a tridomain model for microcirculation of the optic nerve. The model deals with two types of flow: the circulation of water (hydrodynamics) and the circulation of ions (electrodynamics) in the

- glial compartment  $\Omega_{gl}$ .
- axon compartment  $\Omega_{ax}$ .
- extracellular space  $\Omega_{ex}$ .

The interactions between neuronal cells and glial cells have been included in models of the important phenomenon of spreading depression [63-66] thought to be related to epilepsy and migraine. Some two-compartment models for potassium clearance (or spatial buffering) include interactions between neuron cells and extracellular space [67] or interactions between glial cells and extracellular space [68-70]. A tri-compartment model using ordinary differential equations (ODEs) was introduced by Sibille [71] to study the role of  $K_{ir4}$  channels. It shows that the flows play an important role in the central nerve system[72] via influx and efflux routes to

help waste clearance, which has been called (with understandable enthusiasm if not hyperbole) a final frontier of neuroscience [73]. Some models, including flow but not electrodiffusion, were introduced to study the pressure effect on the flow [74-77]. Mori [16] proposed a multidomain model for cortical spreading depression, where ionic electrodiffusion and osmosis between different compartment are considered. We extend those results and present some general conclusions based on the analysis of a specific set of experiments Orkand et al [7, 8] using a model distributed in space in both radial and longitudinal directions and that involves action potentials generated by Hodgkin Huxley equations.

The glial compartment and axon compartment are limited in the optic nerve, while extracellular space exists both in the optic nerve  $\Omega_{ex}^{OP}$  and subarachnoid space  $\Omega_{ex}^{SAS}$ , (See Fig.1)

$$\Omega_{OP} = \Omega_{ax} \cup \Omega_{gl} \cup \Omega_{ex}^{OP}, \quad \Omega_{SAS} = \Omega_{ex}^{SAS}.$$

The model is mainly derived from laws of conservation of ions and water for flow through membranes between intracellular compartments and extracellular space [78]. The field equations themselves have been derived from first principles [23]. It is necessary to derive equations from first principles in composite systems like this in which ‘everything interacts with everything else’. Such derivations guarantee that all equations and variables are consistent. That is to say, all variables satisfy all equations and boundary conditions with one set of unchanging parameters. Deriving field equations for each field individually, and then combining them, is likely to produce inconsistent systems of equations. Inconsistent systems are not only illogical, but they are also likely to yield different results in different research groups, creating discrepancies that are hard to resolve and impede progress towards dealing with important clinical and human problems.

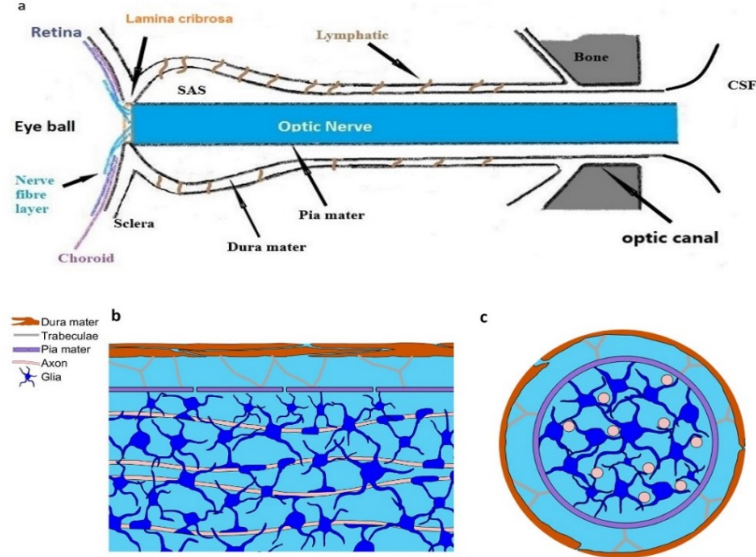


Figure 1: Optic nerve structure. a: Key features of the optic nerve region and subarachnoid space (SAS); b: Longitudinal section of the optic nerve; c: cross section of the optic nerve.

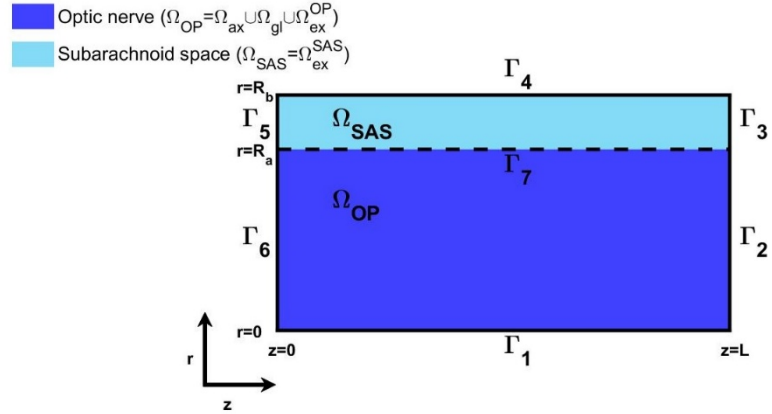


Figure 2: Domain of the axial symmetry model. The optic nerve  $\Omega_{OP}$  consist of axon compartment  $\Omega_{ax}$ , glial compartment  $\Omega_{gl}$  and extracellular space  $\Omega_{ex}^{OP}$ . The subarachnoid space only has extracellular space  $\Omega_{ex}^{SAS}$ .

## 2.1 Notations and Domains

We first introduce the following notations used in the paper, where  $i = \text{Na}^+, \text{K}^+, \text{Cl}^-$  for ion species,  $l = ex, gl, ax$  for extracellular space, glial compartment and axon compartment, and  $k = gl, ax$  for glial or axon membrane in the optic nerve.

$C_l^i$ : Ion  $i$  concentration in the  $l$  region,

$\phi_l$ : Electric potential in  $l$  region,

$P_l$ : Hydrostatic pressure in  $l$  region,

$\mathbf{u}_l$ : Fluid velocity inside of the  $l$  region,

$\eta_l$ : Volume fraction of  $l$  region,

$O_l$ : Osmotic concentration in  $l$  region,

$K_k$ : Stiffness constant of  $k$  membrane,

$\tau_l$ : Tortuosity of  $l$  region,

$z^i$ : Valence of the ion  $i$ ,

$A_l$ : Negative charged protein density in  $l$  region,

$a_k^i$ : Active ATP based ion  $i$  pump on  $k$  membrane,

$b_k^i$ : Passive transmembrane source of  $k$  membrane,

$\mathcal{M}_k$ : Membrane area $k$ in per unit control volume $\Delta V$ ,	$g_k^i$ : Conductance of $k$ membrane for ion $i$ ,
$\kappa_l$ : Water permeability of $l$ region,	$\bar{g}^l$ : Maximum conductance of axon membrane for ion $i$ ,
$L_k^m$ : Membrane hydrostatic permeability of $k$ membrane,	$g_{leak}^i$ : Leak conductance of axon membrane for ion $i$ ,
$\mu$ : Fluid viscosity.	

Fig.1 b shows the model with the whole domain  $\Omega$  that consists of the subarachnoid space (SAS) region  $\Omega_{SAS}$  and optic nerve region  $\Omega_{OP}$  (see Fig. 2),

$$\Omega = \Omega_{SAS} \cup \Omega_{OP},$$

and the interface of two regions is the pia mater denoted by  $\Gamma_7$ ,

$$\Omega_{OP} \cap \Omega_{SAS} = \Gamma_7.$$

In our model, both pia mater  $\Gamma_7$  and dura mater  $\Gamma_4$  are modelled as macroscopic membranes and appropriate boundary conditions. The transmembrane flux of pia mater [79] depends on hydrostatic pressure, osmotic pressure and electric potential, while that of dura mater only depends on the hydrostatic pressure.

Obviously, at higher resolution much more detail will be needed, and these structures will be represented in higher resolution models, in future studies, as the layered epithelia that they are. Higher resolution models will have to be embedded in an overall model of the composite structure if they are to calculate water flow, migration, and diffusion in all three domains: ‘everything depends on everything else’. Coarse graining is not enough: a hierarchy of models will be needed [80]. If higher resolution models are analyzed individually, it will be difficult, if not impossible to join them into a consistent model of the entire system. Different levels of the hierarchy of approximation must be solved together if models are to be consistent and satisfy obligatory conservation laws and Maxwell equations on all scales. If higher resolution models are incorporated into a lower resolution model of the type constructed here, they will be automatically consistent.

For the domain boundaries,  $\Gamma_1$  is the radius center of the optic nerve;  $\Gamma_2$  and  $\Gamma_3$  are the far end (away from the eyeball) of the optic nerve which is connected to optic canal region [81].  $\Gamma_5$  is used to model the dura mater connected to sclera (the white matter of the eye) and assumed to be non-permeable [82].  $\Gamma_6$  is used to denote the the lamina cribrosa where the optic nerve head exits the eye posteriorly through pores of the lamina cribrosa [83].

In the optic nerve region  $\Omega_{OP}$ , the glial membrane and axon membrane separate domains  $\Omega_{gl}$ ,  $\Omega_{ax}$  from the extracellular region  $\Omega_{ex}^{OP}$ , respectively (also see Fig. 1).

Based on the structure of optic nerve, we have the following global assumptions for the model:

- **Isotropy of glia and extracellular regions:**

- 1) The extracellular space forms a narrow structure of branching clefts surrounding the glial cells and nerve axons.
- 2) The glial cells are connected to each other by connexins and form a syncytium.
- 3) The extracellular space is continuous and forms a syncytium.

Both syncytia are assumed isotropic here, until we know better. The axons are not connected to each other. For  $l = gl, ex, i = \text{Na}^+, \text{K}^+, \text{Cl}^-$ , the ion flux and water flow velocity are in the following forms

$$J_l^i = J_{l,r}^i \hat{\mathbf{r}} + J_{l,\theta}^i \hat{\boldsymbol{\theta}} + J_{l,z}^i \hat{\mathbf{z}}, \quad (2.1)$$

$$\mathbf{u}_l = u_l^r \hat{\mathbf{r}} + u_l^\theta \hat{\boldsymbol{\theta}} + u_l^z \hat{\mathbf{z}}. \quad (2.2)$$

- **Anisotropy of axon region:** The axons are separate, more or less parallel cylindrical cells that do not form a syncytium. For  $i = \text{Na}^+, \text{K}^+, \text{Cl}^-$ , the ion flux and water flow velocity are in the following forms

$$J_{ax}^i = J_{ax,z}^i \hat{\mathbf{z}}, \quad (2.3)$$

$$\mathbf{u}_{ax} = u_{ax}^z \hat{\mathbf{z}}. \quad (2.4)$$

- **Charge neutrality:** In each domain, we assume electroneutrality.

$$\eta_{gl} \sum_i z^i C_{gl}^i + z^{gl} A_{gl} \eta_{gl}^{re} = 0, \quad (2.5)$$

$$\eta_{ax} \sum_i z^i C_{ax}^i + z^{ax} A_{ax} \eta_{ax}^{re} = 0, \quad (2.6)$$

$$\sum_i z^i C_{ex}^i = 0, \quad (2.7)$$

where  $A_l > 0$  with  $l = ax, gl$  is the density of proteins in axons or glial cells. The proteins have negative charge, but the charge density is customarily described by a positive number. The  $\eta_{ax}$  and  $\eta_{gl}$  are the volume fraction of axon and glial compartments in optic nerve and  $\eta_{ax}^{re}$  and  $\eta_{gl}^{re}$  are the resting state volume fraction of axon and glial compartments in optic nerve.

- **Axis symmetry:** For simplicity, axial symmetry is assumed. The model can be straightforwardly extended to full three dimensions when data and needs justify the considerable extra computational resources needed to analyze such models.

## 2.2 Water Circulation

We model water circulation with the following assumptions

- the loss of water in axons and glial cells is only through membranes flowing into or out of the extracellular space.
- the transmembrane water flux is proportional to the intra/extracellular hydrostatic pressure and osmotic pressure differences.
- the glial cell and axons could swell and shrink due to the water inflows and

outflows.

If we use  $\eta_l$  to describe the volume fraction of  $l$  region ( $l = gl, ax, ex$ ), then conservation of mass in each domain yields

$$\frac{\partial \eta_{gl}}{\partial t} + \mathcal{M}_{gl} L_{gl}^m (P_{gl} - P_{ex} - \gamma_{gl} k_B T (O_{gl} - O_{ex})) + \nabla \cdot (\eta_{gl} \mathbf{u}_{gl}) = 0, \text{ in } \Omega_{OP} \quad (2.8)$$

$$\frac{\partial \eta_{ax}}{\partial t} + \mathcal{M}_{ax} L_{ax}^m (P_{ax} - P_{ex} - \gamma_{ax} k_B T (O_{ax} - O_{ex})) + \frac{\partial}{\partial z} (\eta_{ax} u_{ax}^z) = 0, \text{ in } \Omega_{OP} \quad (2.9)$$

$$\nabla \cdot (\eta_{gl} \mathbf{u}_{gl}) + \nabla \cdot (\eta_{ex} \mathbf{u}_{ex}) + \frac{\partial}{\partial z} (\eta_{ax} u_{ax}^z) = 0, \text{ in } \Omega_{OP} \quad (2.10)$$

where we assume that glial cells are isotropic, and axons are anisotropic. Here  $\mathbf{u}_l$  and  $P_l$  with  $l = gl, ax, ex$  are the velocity and pressure in the glial cells and axons and extracellular space, respectively. And  $k_B T O_l$  is the osmotic [23, 51] defined by

$$O_{ex} = \sum_i C_{ex}^i, \quad O_l = \sum_i C_l^i + A_l \frac{\eta_l^{re}}{\eta_l}, \quad l = gl, ax,$$

where  $A_l \frac{\eta_l^{re}}{\eta_l} > 0$  is the density of the permanent negatively charged protein in glial cells and axons that varies with the volume (fraction) of the region. In this paper, we assume the permanent negatively charged protein is uniformly distributed within glial cells and axons and has valence  $z^l$ ,  $l = gl, ax$ . The  $\mathcal{M}_l$  and  $\gamma_l$ ,  $l = gl, ax$  are the glial cells (or axons) membrane area per unit volume and membrane reflection coefficient [84] respectively. The membrane reflection coefficient  $\gamma_l$  is the ratio between the observed osmotic pressure and theoretical osmotic pressure.  $k_B$  is Boltzmann constant and  $T$  is temperature.

For the volume fraction  $\eta_l$ ,  $l = ax, gl, ex$ , we have

$$\eta_{gl} + \eta_{ax} + \eta_{ex} = 1, \quad \text{in } \Omega. \quad (2.11)$$

**Remark 2.1** Note the glial cells and axons are found only in the  $\Omega_{OP}$  region. In other words,  $\eta_{ax} = \eta_{gl} \equiv 0$  and  $\eta_{ex} \equiv 1$  are fixed in  $\Omega_{SAS}$ . Therefore, the solution is incompressible in the  $\Omega_{SAS}$  and we have

$$\nabla \cdot (\eta_{ex} \mathbf{u}_{ex}) = 0. \quad (2.12)$$

The relation between the hydrostatic pressure  $P_l$  and volume fraction  $\eta_l$  ( $l = ex, gl, ax$ ) is connected by the force balance on the membrane  $\mathcal{M}_k$  ( $k = gl, ax$ ) [16, 23]

$$K_{gl} (\eta_{gl} - \eta_{gl}^{re}) = P_{gl} - P_{ex} - (P_{gl}^{re} - P_{ex}^{re}), \quad \text{in } \Omega_{OP} \quad (2.13)$$

$$K_{ax} (\eta_{ax} - \eta_{ax}^{re}) = P_{ax} - P_{ex} - (P_{ax}^{re} - P_{ex}^{re}), \quad \text{in } \Omega_{OP} \quad (2.14)$$

where  $K_{gl,ax}$  is the stiffness constant and  $\eta_l^{re}$  and  $P_l^{re}$  ( $l = ex, gl, ax$ ) are the resting state volume fraction and hydrostatic pressure.

Note that the concentrations of ions and effective concentration of water vary a great deal and so are described by equations in which the number density of ions and effective number density of water vary in both the radial and longitudinal directions according to conservation laws, without using compartments that may not have unique definitions or relations to anatomical structures. Indeed, the variation of concentration is one of the main determinants of the properties of ionic solutions. The solution is incompressible, the components are not [25].

Next, we define the velocity in each domain.

**Water Velocities in the Glial Compartment.** As we mentioned before, the glial space is a connected space, where water can flow from cell to cell through connexin proteins joining membranes of neighboring cells. The velocity of fluid in glial syncytium  $\mathbf{u}_{gl}$  depends on the gradients of hydrostatic pressure and osmotic pressure:

$$u_{gl}^r = -\frac{\kappa_{gl}\tau_{gl}}{\mu} \left( \frac{\partial P_{gl}}{\partial r} - \gamma_{gl}k_B T \frac{\partial \sigma_{gl}}{\partial r} \right), \quad (2.15)$$

$$u_{gl}^\theta = -\frac{\kappa_{gl}\tau_{gl}}{\mu} \left( \frac{1}{r} \frac{\partial P_{gl}}{\partial \theta} - \gamma_{gl}k_B T \frac{1}{r} \frac{\partial \sigma_{gl}}{\partial \theta} \right), \quad (2.16)$$

$$u_{gl}^z = -\frac{\kappa_{gl}\tau_{gl}}{\mu} \left( \frac{\partial P_{gl}}{\partial z} - \gamma_{gl}k_B T \frac{\partial \sigma_{gl}}{\partial z} \right). \quad (2.17)$$

The boundary conditions of fluid in the glial syncytium are as follows

$$\begin{cases} \mathbf{u}_{gl} \cdot \hat{\mathbf{r}} = 0, & \text{on } \Gamma_1 \\ \nabla P_{gl} \cdot \hat{\mathbf{z}} = 0, & \text{on } \Gamma_2 \\ \nabla P_{gl} \cdot \hat{\mathbf{z}} = 0, & \text{on } \Gamma_6 \\ \mathbf{u}_{gl} \cdot \hat{\mathbf{r}} = 0, & \text{on } \Gamma_7 \end{cases} \quad (2.18)$$

- (1) At boundary  $\Gamma_2$  and  $\Gamma_6$ , the homogeneous Neumann boundary condition is applied.
- (2) Non-flux boundary condition is used at  $\Gamma_7$ .

**Water Velocity in the Axon Compartment.** Since the axons are only connected in the longitudinal direction, the fluid velocity in axons region is defined along  $z$  direction as

$$u_{ax}^r = 0, \quad (2.19)$$

$$u_{ax}^\theta = 0, \quad (2.20)$$

$$u_{ax}^z = -\frac{\kappa_{ax}}{\mu} \frac{\partial P_{ax}}{\partial z}, \quad (2.21)$$

Dirichlet boundary conditions are used to the fluid velocity in axons

$$\begin{cases} \mathbf{u}_{ax} \cdot \hat{\mathbf{z}} = u_{0l}, & \text{on } \Gamma_2 \\ \mathbf{u}_{ax} \cdot \hat{\mathbf{z}} = u_{0r}, & \text{on } \Gamma_6 \end{cases} \quad (2.22)$$

where  $u_{0l}$  and  $u_{0r}$  are inflow and outflow velocities at  $\Gamma_6$  and  $\Gamma_2$ , respectively.

**Velocity in the Extracellular Space.** The extracellular space is narrow, and the extracellular velocity is determined by the gradients of hydrostatic pressure and electric potential

$$u_{ex}^r = -\frac{\kappa_{ex}\tau_{ex}}{\mu} \frac{\partial P_{ex}}{\partial r} - k_e \tau_{ex} \frac{\partial \phi_{ex}}{\partial r}, \quad (2.23)$$

$$u_{ex}^\theta = -\frac{\kappa_{ex}\tau_{ex}}{\mu} \frac{1}{r} \frac{\partial P_{ex}}{\partial \theta} - k_e \tau_{ex} \frac{1}{r} \frac{\partial \phi_{ex}}{\partial \theta}, \quad (2.24)$$

$$u_{ex}^z = -\frac{\kappa_{ex}\tau_{ex}}{\mu} \frac{\partial P_{ex}}{\partial z} - k_e \tau_{ex} \frac{\partial \phi_{ex}}{\partial z}, \quad (2.25)$$

where  $\phi_{ex}$  is the electric potential in the extracellular space,  $\tau_{ex}$  is the tortuosity of extracellular region [78, 85] and  $\mu$  is the viscosity of water,  $k_e$  is introduced to describe the effect of electro-osmotic flow [45, 55, 86],  $\kappa_{ex}$  is the permeability of intracellular region ( $l = in$ ) and extracellular region ( $l = ex$ ), respectively. Here the hydro permeability  $\kappa_{ex}$ ,  $\tau_{ex}$  and electric osmotic  $k_e$  have two distinguished values in the region  $\Omega_{ex}^{OP}$  and  $\Omega_{ex}^{SAS}$ .

$$\kappa_{ex} = \begin{cases} \kappa_{ex}^{OP}, & \text{in } \Omega_{ex}^{OP}, \\ \kappa_{ex}^{SAS}, & \text{in } \Omega_{ex}^{SAS}, \end{cases} \quad \tau_{ex} = \begin{cases} \tau_{ex}^{OP}, & \text{in } \Omega_{ex}^{OP}, \\ \tau_{ex}^{SAS}, & \text{in } \Omega_{ex}^{SAS}, \end{cases} \quad k_e = \begin{cases} k_e^{OP}, & \text{in } \Omega_{ex}^{OP}, \\ k_e^{SAS}, & \text{in } \Omega_{ex}^{SAS} \end{cases} \quad (2.26)$$

Since  $\Gamma_2 \cup \Gamma_3$  are the far end of optic nerve away from eyeball and next to connect to optic canal, we assume the hydrostatic pressure of extracellular is equal to the cerebrospinal fluid pressure. On the other hand, the intraocular pressure (IOP) is imposed at  $\Gamma_6$  where the extracellular space is connected to the retina. At boundary  $\Gamma_5$ , we assume a non-permeable boundary. We are aware of the significance of the pressures and flows at these boundaries for clinical phenomena including glaucoma [57, 77, 87, 88] and will return to that subject in later publications.

The water flow across the semi-permeable membrane  $\Gamma_4$  is produced by the lymphatic drainage on the dura membrane, which depends on the difference between extracellular pressure and orbital pressure (OBP). We assume the velocity across the pia membrane  $\Gamma_4$ , is continuous and determined by the hydrostatic pressure and osmotic pressure. To summarize, the boundary conditions of the extracellular fluid are

$$\begin{cases} \mathbf{u}_{ex} \cdot \hat{\mathbf{r}} = 0, \\ P_{ex} = P_{CSF}, \\ \mathbf{u}_{ex}^{SAS} \cdot \hat{\mathbf{r}} = L_{dr}^m (P_{ex}^{SAS} - P_{OBP}), \\ \mathbf{u}_{ex} \cdot \hat{\mathbf{r}} = 0, \\ P_{ex} = P_{ICP}, \\ \mathbf{u}_{ex}^{OP} \cdot \hat{\mathbf{r}} = \mathbf{u}_{ex}^{SAS} \cdot \hat{\mathbf{r}} = L_{pia}^m (P_{ex}^{OP} - P_{ex}^{SAS} - \gamma_{pia} k_B T (O_{ex}^{OP} - O_{ex}^{SAS})), \end{cases} \quad (2.27)$$

where  $P_{CSF}$  is the cerebrospinal fluid pressure [77] and  $P_{ICP}$  is the pressure in eye and  $P_{OP}$  is the orbital pressure on the dura mater.

## 2.3 Ion Transport

For ion circulation, we assume

- Only three types of ions are considered:  $K^+$ ,  $Na^+$  and  $Cl^-$ .
- The sodium-potassium ATP pump is present in both glial and axon membranes.
- Ion channel conductance in glial cell membranes is a fixed constant, independent of voltage and time. The sodium conductance is assumed small and its channel origin unknown. The potassium conductance is large and comes from the  $K_{ir4}$  channels [72, 89].
- Sodium and potassium channels conductance on axons are potential dependent, while the chloride channel conductance is fixed.

The conservation of ion concentration implies the following system of partial differential equations to describe the dynamics of ions in each region, for  $i = Na^+, K^+, Cl^-$

$$\frac{\partial(\eta_{gl}C_{gl}^i)}{\partial t} + \mathcal{M}_{gl}(a_{gl}^i + b_{gl}^i) + \nabla \cdot (\eta_{gl}\mathbf{J}_{gl}^i) = 0, \quad \text{in } \Omega_{OP}, \quad (2.28)$$

$$\frac{\partial(\eta_{ax}C_{ax}^i)}{\partial t} + \mathcal{M}_{ax}(a_{ax}^i + b_{ax}^i) + \frac{\partial}{\partial z}(\eta_{ax}J_{ax,z}^i) = 0, \quad \text{in } \Omega_{OP}, \quad (2.29)$$

$$\frac{\partial(\eta_{ex}C_{ex}^i)}{\partial t} - \mathcal{M}_{ax}(a_{ax}^i + b_{ax}^i) - \mathcal{M}_{gl}(a_{gl}^i + b_{gl}^i) + \nabla \cdot (\eta_{ex}\mathbf{J}_{ex}^i) = 0, \quad \text{in } \Omega_{OP}, \quad (2.30)$$

where the last equation reduces to the following in the  $\Omega_{SAS}$  region,

$$\frac{\partial C_{ex}^{SAS}}{\partial t} + \nabla \cdot \mathbf{J}_{ex}^{i,SAS} = 0. \quad (2.31)$$

Here  $a_l^i$  is the active  $Na/K$  pump effect and  $b_l^i$  is passive source for ion  $i$  on the axons ( $l = ax$ ) or glial cells membranes ( $l = gl$ ). In the glial cell membranes,  $b_{gl}^i$  is defined as

$$b_{gl}^i = \frac{g_{gl}^i}{z^i e} (\phi_{gl} - \phi_{ex} - E_{gl}^i), \quad (2.32)$$

where the Nernst potential is used to describe the gradient of chemical potential  $E_{gl}^i = \frac{k_B T}{e z^i} \log \left( \frac{C_{ex}^i}{C_{gl}^i} \right)$  and the conductance  $g_{gl}^i$  for each ion in the glial membrane is a fixed constant, independent of voltage and time. On the axon's membrane,  $b_{ax}^i$  is defined as

$$b_{ax}^i = \frac{g_{ax}^i}{z^i e} (\phi_{ax} - \phi_{ex} - E_{ax}^i), \quad (2.33)$$

where

$$\begin{aligned} g_{ax}^{Na} &= \bar{g}^{Na} m^3 h + g_{leak}^{Na}, \\ g_{ax}^K &= \bar{g}^K n^4 + g_{leak}^K, \end{aligned}$$

and the time dependent dynamic of open probability, often loosely called ‘gating’ is governed by the Hodgkin-Huxley model [90, 91]

$$\begin{aligned} \frac{dn}{dt} &= \alpha_n(1 - n) - \beta_n n, \\ \frac{dm}{dt} &= \alpha_m(1 - m) - \beta_m m, \\ \frac{dh}{dt} &= \alpha_h(1 - h) - \beta_h h, \end{aligned} \quad (2.34)$$

We assume that the only pump is the Na/K active transporter. We are more than aware that other active transport systems can and likely do move ions and water in this system. They will be included as experimental information becomes available.

In the case of the Na/K pump  $a_l^i$ ,  $l = ax, gl$ , the strength of the pump depends on the concentration in the intracellular and extracellular space [90, 92], i.e.

$$a_l^{Na} = 3 \frac{I_l}{e}, \quad a_l^K = -2 \frac{I_l}{e}, \quad a_l^{Cl} = 0, \quad l = ax, gl, \quad (2.35)$$

where

$$I_l = I_{l,1} \left( \frac{C_l^{Na}}{C_l^{Na} + K_{Na1}} \right)^3 \left( \frac{C_{ex}^K}{C_{ex}^K + K_{K1}} \right)^2 + I_{l,2} \left( \frac{C_l^{Na}}{C_l^{Na} + K_{Na2}} \right)^3 \left( \frac{C_{ex}^K}{C_{ex}^K + K_{K2}} \right)^2, \quad (2.36)$$

$I_{l,1}$  and  $I_{l,2}$  are related to  $\alpha_1$  – and  $\alpha_2$  – isoform of Na/K pump.

The definitions of ion flux in each domain is are as follows, for  $i = \text{Na}^+, \text{K}^+, \text{Cl}^-$ ,

$$\mathbf{J}_l^i = C_l^i \mathbf{u}_l - D_{gl}^i \tau_l \left( \nabla C_l^i + \frac{z^i e}{k_B T} C_l^i \nabla \phi_l \right), \quad l = gl, ex, \quad (2.37)$$

$$J_{ax,z}^i = C_{ax}^i u_{ax}^z - D_{ax}^i \left( \frac{\partial C_{ax}^i}{\partial z} + \frac{z^i e}{k_B T} C_{ax}^i \frac{\partial \phi_{ax}}{\partial z} \right). \quad (2.38)$$

For the axon compartment and glial compartment boundary condition, we have

$$C_{ax}^i = C_{ax}^{i,re}, \quad \text{on } \Gamma_2 \cup \Gamma_6, \quad (2.39)$$

and

$$\begin{cases} \mathbf{J}_{gl}^i \cdot \hat{\mathbf{r}} = 0, & \text{on } \Gamma_1, \\ C_{gl}^i = C_{gl}^{i,re}, & \text{on } \Gamma_2 \cup \Gamma_6, \\ \mathbf{J}_{gl}^i \cdot \hat{\mathbf{r}} = 0, & \text{on } \Gamma_7, \end{cases} \quad (2.40)$$

where the Dirichlet boundary conditions are used at locations  $\Gamma_2 \cup \Gamma_6$  for axons and glial cell membranes, and a non-flux boundary condition is used for glial cells ions flux on pia mater  $\Gamma_7$ .

For the extracellular space boundary condition, similar boundary conditions are imposed except on the pia mater  $\Gamma_7$ . The flux across the pia mater is assumed continuous and Ohm's law is used [51]. Additionally, a non-permeable boundary condition is used at location  $\Gamma_5$  and a homogeneous Neumann boundary condition is applied at the location of the dura mater  $\Gamma_4$ ,

$$\left\{ \begin{array}{ll} \mathbf{J}_{ex}^i \cdot \hat{\mathbf{r}} = 0, & \text{on } \Gamma_1, \\ C_{ex}^i = C_{csf}^i, & \text{on } \Gamma_2 \cup \Gamma_3, \\ \nabla C_{ex}^i \cdot \hat{\mathbf{r}} = 0, & \text{on } \Gamma_4, \\ \mathbf{J}_{ex}^i \cdot \hat{\mathbf{z}} = 0, & \text{on } \Gamma_5, \\ C_{ex}^i = C_{eye}^i, & \text{on } \Gamma_6, \\ \mathbf{J}_{ex}^{i,OP} \cdot \hat{\mathbf{r}} = \mathbf{J}_{ex}^{i,SAS} \cdot \hat{\mathbf{r}} = \frac{C_{pia}^i}{z^i e} (\phi_{ex}^{OP} - \phi_{ex}^{SAS} - E_{pia}^i), & \text{on } \Gamma_7, \end{array} \right. \quad (2.41)$$

Multiplying equations in (2.28-2.30) with  $z^i e$  respectively, summing up, and using equation (2.5-2.7) we have following system for the electric fields in  $ax, gl, ex$ ,

$$\sum_i z^i e \mathcal{M}_{gl} (\alpha_{gl}^i + \beta_{gl}^i) + \sum_i z^i e \nabla \cdot (\eta_{gl} \mathbf{J}_{gl}^i) = 0, \quad (2.42)$$

$$\sum_i z^i e \mathcal{M}_{ax} (\alpha_{ax}^i + \beta_{ax}^i) + \sum_i z^i e \frac{\partial}{\partial z} (\eta_{ax} \mathbf{J}_{ax,z}^i) = 0, \quad (2.43)$$

$$\sum_i z^i e \nabla \cdot (\eta_{gl} \mathbf{J}_{gl}^i) + \sum_i z^i e \frac{\partial}{\partial z} (\eta_{ax} \mathbf{J}_{ax,z}^i) + \sum_i z^i e \nabla \cdot (\eta_{ex} \mathbf{J}_{ex}^i) = 0. \quad (2.44)$$

In the subarachnoid space  $\Omega_{SAS}$ , the extracellular equations reduce to

$$\sum_i z^i e \nabla \cdot (\sum_i \mathbf{J}_{ex}^{i,SAS}) = 0. \quad (2.45)$$

The boundary condition for electric fields  $\phi_{ax}, \phi_{gl}$  and  $\phi_{ex}$  are  
In the axon compartment:

$$\left\{ \begin{array}{ll} \nabla \phi_{ax} \cdot \hat{\mathbf{z}} = 0, & \text{on } \Gamma_2, \\ \nabla \phi_{ax} \cdot \hat{\mathbf{z}} = 0, & \text{on } \Gamma_6. \end{array} \right. \quad (2.46)$$

In the glial compartment:

$$\left\{ \begin{array}{ll} \phi_{gl} \cdot \hat{\mathbf{r}} = 0, & \text{on } \Gamma_1, \\ \nabla \phi_{gl} \cdot \hat{\mathbf{z}} = 0, & \text{on } \Gamma_2, \\ \nabla \phi_{gl} \cdot \hat{\mathbf{z}} = 0, & \text{on } \Gamma_6, \\ \sum_i z^i e \mathbf{J}_{gl}^i \cdot \hat{\mathbf{r}} = 0, & \text{on } \Gamma_7, \end{array} \right. \quad (2.47)$$

and in the extracellular space:

$$\left\{ \begin{array}{ll} \sum_i z^i e \mathbf{J}_{ex}^i \cdot \hat{\mathbf{r}} = 0, & \text{on } \Gamma_1, \\ \nabla \phi_{ex} \cdot \hat{\mathbf{z}} = 0, & \text{on } \Gamma_2 \cup \Gamma_3, \\ \nabla \phi_{ex} \cdot \hat{\mathbf{r}} = 0, & \text{on } \Gamma_4, \\ \sum_i z^i e \mathbf{J}_{ex}^i \cdot \hat{\mathbf{z}} = 0, & \text{on } \Gamma_5, \\ \nabla \phi_{ex} \cdot \hat{\mathbf{z}} = 0, & \text{on } \Gamma_6, \\ \sum_i z^i e \mathbf{J}_{ex}^{i,OP} \cdot \hat{\mathbf{r}} = \sum_i z^i e \mathbf{J}_{ex}^{i,SAS} \cdot \hat{\mathbf{r}} = \sum_i G_{pia}^i (\phi_{ex}^{OP} - \phi_{ex}^{SAS} - E_{pia}^i), & \text{on } \Gamma_7. \end{array} \right. \quad (2.48)$$

### 3. Model Calibration

Our work is possible because of, and was motivated by the paper of Orkand et al [7, 8] that measured the accumulation of potassium in the narrow extracellular space of the optic nerve of the amphibian salamander *Necturus*, in the spirit of the original work of Frankenhaeuser and Hodgkin [4], that first analyzed accumulation of potassium outside a nerve fiber. The existence and qualitative properties of that accumulation of potassium were known to, and a cause for concern for Hodgkin, from his first work on the voltage clamp [1, 2], if not earlier. Hodgkin described the phenomena as part of what was called [concentration] ‘polarization’ and discussed it extensively with students sometime later (Eisenberg, personal communication, ~1962)

The key experiment in the Orkand paper [8] measures the change in potential across the glial membrane produced by a train of action potentials. The glial membrane potential is used to estimate and report the potassium concentration in the narrow extracellular space, because the glial membrane is populated with more or less voltage independent potassium channels and not much else.

In the experiment, optic nerve has been put in three different  $K^+$  concentrations (1.5 mM, 3 mM, 4.5 mM) in the bathing solution to change the resting potential across the glia membrane. Then the axon was stimulated to give a train of action potentials. The action potentials increased  $K^+$  in extracellular space (ECS). The accumulated  $K^+$  then made the glia membrane potential more positive. Stimuli were applied at both ends of a region of the optic nerve thereby producing a more uniform (in space) potential within that region.

In our simulation study, we first set concentration in ECS  $K^+$  to be 3 mM and obtained a resting potential across the glia membrane  $\sim -89$  mV. In Orkand’s work [7, 8], for recording and stimulating, the two ends of the optic nerve were placed in suction electrodes (we applied a train of current though the axon membrane at  $z = 1.5$  mm, 13.5 mm,  $0 < r < R_a = r^* = 48$   $\mu$ m). Each stimulus lasted 3 ms (as Orkand’s paper indicated) and with strength 3 mA/m<sup>2</sup> which is big enough for passing threshold and generating an action potential. After a train of stimulus with frequency 17/s for 1s, the first panel of Fig. (3.1) shows the train of axon membrane action potentials and its return to baseline ( $\sim -89$  mV) after 1s at the point  $r = 0$  and  $z = L/2$ . The profiles of the first action potential and last action potential in the

train are presented in the second panel. The third and fourth panels are used to illustration the increasements of glial cell membrane potential and extracellular potassium concentration during and after the train of stimulus. The figure shows that during the stimulus, the ECS  $K^+$  concentration keeps increasing due to the opening of the voltage gated potassium channel of the axon membrane. Due to the accumulation of ECS  $K^+$ , the membrane potential of glial cells also keeps increasing (becoming more positive) until the stimulus stops.

Then, we vary the ECS  $K^+$  to be 1.5 mM, 3 mM, 4.5 mM and record the magnitude of the maximum glial membrane depolarized potential in each case as in the Fig. (3.2). The black symbols are used for experimental data, blue ones are the simulations results of our model, respectively. Fig. 3.2 shows that our model could match the experimental resting potentials (solid symbols) and depolarization potentials (open symbols) very well with different ECS  $K^+$  concentrations.

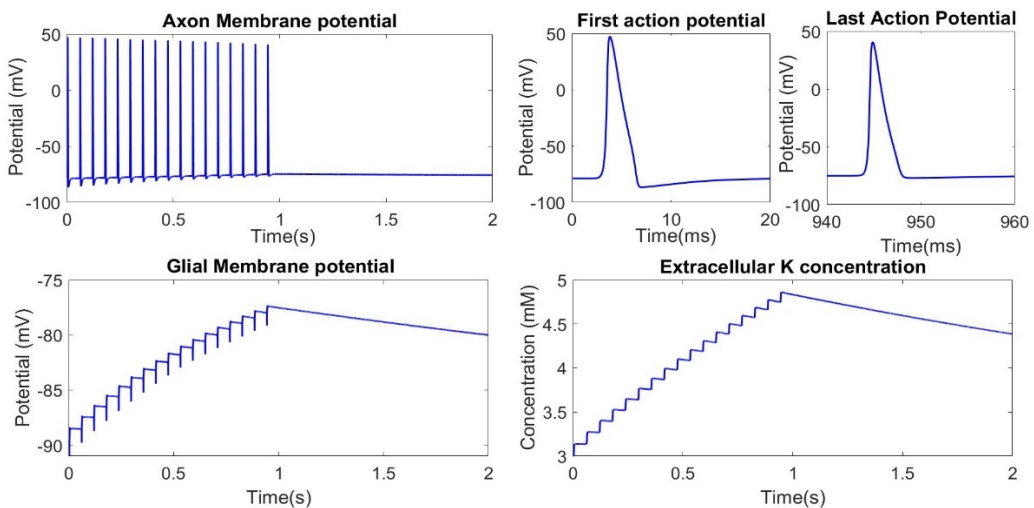


Figure 3.1: When the extracellular solution with 3 mM  $K^+$ , the records of axon membrane potential, glial membrane potential and extracellular  $K^+$  at center axis point.

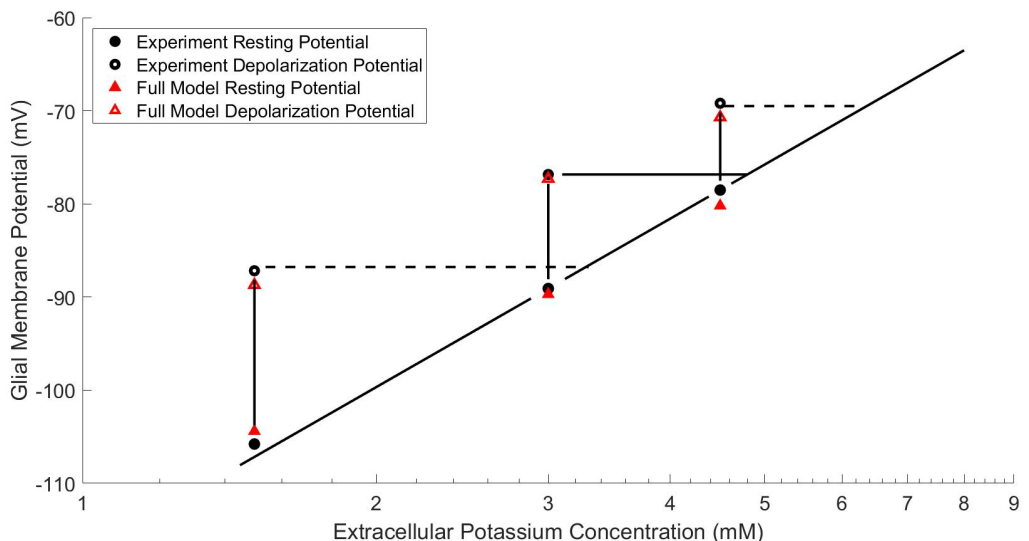


Figure 3.2: The comparison between the experiment in [8] and simulation on the effect of nerve impulses on the membrane potential of glial cells. The solid symbols are resting potentials and the open symbols are depolarization potentials with different ECS  $K^+$  concentrations.

## 4. Potassium clearance

In this section, we make comparisons of the potassium clearance under various conditions based on the full model. In the section 4.1, we focus on applying the stimuli at alternative locations on the axon. We show how the cooperation between the extracellular pathway and glial transmembrane pathway helps potassium clearance. In section 4.2, we have a glimpse of the effect of the glial membrane conductance changes as well as variations in the pia mater boundary conditions. We introduce the NKCC channel into the glial membrane and a non-selective pathway on the pia mater and compare the potassium clearance with the baseline model.

### 4.1 Alternative Distribution of Stimulus Location

In this section, current is applied at several different radial locations. We wondered whether the choice radial location would change our calculations of potassium clearance and fluid velocity.

To facilitate the discussion on the cooperation between extracellular pathway and glial transmembrane pathway for  $K^+$  clearance, we define the following regions which potassium flux could pass through,

$M_S$ : Glial transmembrane in stimulated region.

$E_T$ : Extracellular pathway in transition region.

$M_{NS}$ : Glial Transmembrane in non-stimulated region.

$G_T$ : Glial pathway in transition region.

We mainly focus on the two distinguished periods of time, (1) during a train of axon firing  $([0, T_{sti}])$  (2) after axon firing  $([T_{sti}, T_{af}])$  when the axon stops stimulated.

In the simulations below, we take  $T_{sti} = 0.2$  s and  $T_{af} = 10$  s.

#### 4.1.1 Inner and Outer radial regions stimulated

We first make a comparison between the inner radial region stimulated which the current applied on  $S_{sti}^{in} (= \{(r, z) | r < \frac{r^*}{2}, z = z_0\})$  and outer radial region stimulated which  $S_{sti}^{out} (= \{(r, z) | \frac{r^*}{2} < r < r^*, z = z_0\})$ . Since the axon signal propagate in  $z$  direction, for the inner radial region stimulated case, the stimulated region is  $V_s^{in} = \{(r, z) | r < \frac{r^*}{2}, z \in [0, L]\}$  and the non-stimulated region is

$V_{ns}^{in} = \{(r, z) \mid \frac{r^*}{2} < r < r^*, z \in [0, L]\}$ ; for the outer radial region stimulated case,

$V_s^{out} = V_{ns}^{in}$  and  $V_{ns}^{out} = V_s^{in}$ . The transition region  $S_t = \{(r, z) \mid r = \frac{r^*}{2}, z \in [0, L]\}$  is the same for both cases.

### (a) During a train of neuron firing

In the Fig. 4.1, we show the total potassium flux (potassium flux integrated over area) and cumulative potassium flux (total potassium flux integrated over time) during axon firing period  $[0, T_{sti}]$ . In both cases, the figures show that the transmembrane flow from extracellular to glial and the communication inside the extracellular act together to help the potassium clearance. The strength of fluxes is gradually increased during axon firing period as in Fig. 4.1a&b. It confirms that the potassium flux during stimulus is still flow from the stimulus region to the non-stimulus region, in both the extracellular space and glial compartment. The cumulative potassium flux through the glial membrane ( $M_S$ ) is twice as large as that through the extracellular pathway in transition region ( $E_T$ ) as shown in Fig. 4.1e&f.

The glial compartment serves as an important and quick potassium transport device to remove potassium accumulated while the neuron fires action potentials. In the stimulated region, the accumulated potassium makes the potassium Nernst potential more positive. The change in the potassium Nernst potential induces potassium movement into the glial compartment from extracellular space (Fig. 4.1a). This inflow makes the glial compartment electric potential more positive and moves potassium ions from the stimulated region to the unstimulated region (Fig. 4.1d). In the unstimulated region, the glial membrane potential also becomes more positive as it does in the stimulated region because the glia is an electrical syncytium in the longitudinal and radial directions. However, the glial potassium Nernst potential in the unstimulated region is not very different from that in the resting state. These potentials produce the outward potassium flux from the glial compartment in the unstimulated region (Fig. 4.1c). Interacting regions of this sort depend on spatial variables and the properties of the glia as a syncytium in the longitudinal as well as radial directions. It is difficult to capture these effects in models that do not include radial and longitudinal directions as independent variables. The schematic graph of potassium circulation in the optic nerve is summarized in the Fig. 4.3a.

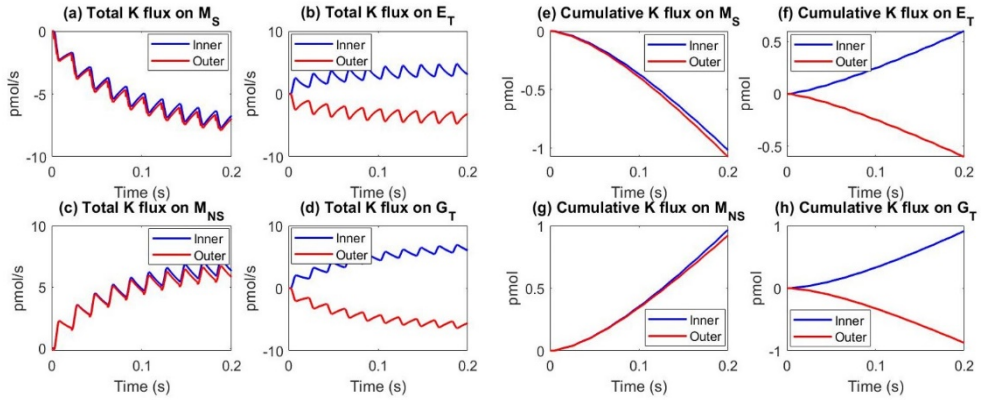


Figure 4.1 a-d: potassium flux through  $M_S$ ,  $E_T$ ,  $M_{NS}$  and  $G_T$  during a train of axon firing (glial membrane flux with normal direction pointing to ECS, transition region in ECS and glial compartment with normal direction is radial direction). e-h: cumulative potassium flux during axon firing period  $[0, T_{sti}]$ .

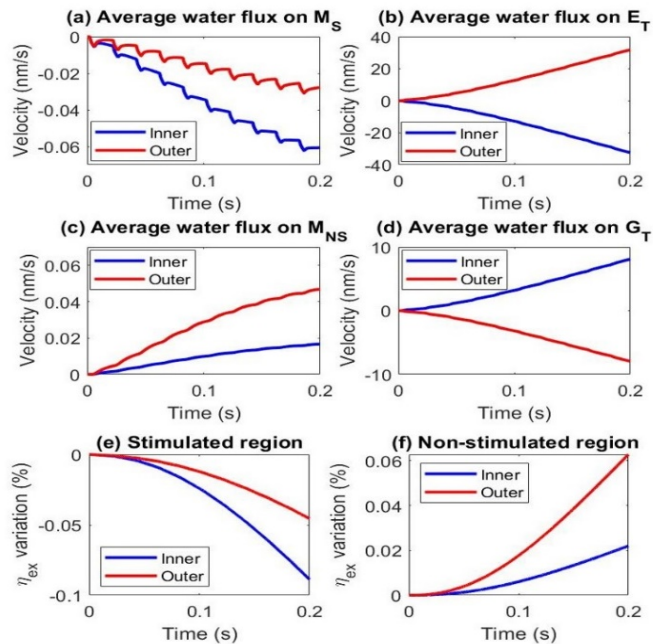


Figure 4.2 a-d: Average water velocity through  $M_S$ ,  $E_T$ ,  $M_{NS}$  and  $G_T$  during a train of axon firing period  $[0, T_{sti}]$ . e-f: the extracellular volume fraction variation in the stimulated region and non-stimulated region.

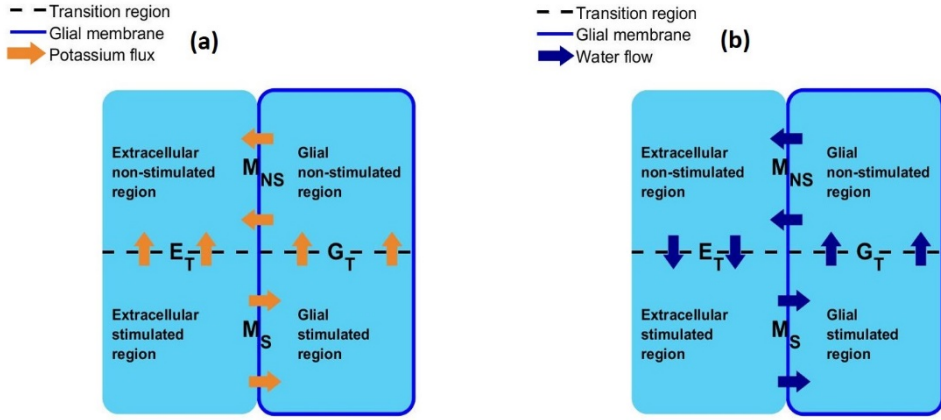


Figure 4.3 a: Schematic graph of the potassium flux when axon is stimulated. In the stimulated region, the potassium moves through the extracellular pathway and through the glial compartment by way of the glial membrane. In the non-stimulated region, the potassium leaks out to the extracellular space through the glial membrane. b: Schematic graph of the water circulation when the inner part of the axon is stimulated. In the stimulated region, the glial transmembrane water flow goes from extracellular space into glial compartment as the effect of osmosis difference. In the extracellular space, water goes from non-stimulated region to stimulated region in the radial direction. In the glia compartment goes in the opposite direction. Note these graphs are graphs that summarize outputs of large numbers of calculations solving partial differential equations in longitudinal and radial spatial directions and time. They do not represent a compartmental model. They are the output of a model distributed in space.

The water circulation in the optic nerve is driven by the gradient of osmotic pressure in the stimulated region. In the stimulated region, the extracellular osmotic pressure  $k_B T O_{ex}$  decreased, and glial compartment osmotic flow of water is increased. This is because there is more potassium flux moving into the glial compartment through the glial membrane, but a smaller amount of sodium flux out of the glial compartment because of the ion channel conductance difference between the potassium and sodium channels in the glial membrane. In the glial compartment in the stimulated region of the optic nerve fiber, there is an increase in the water flux into the glial compartment from the extracellular space (Fig. 4.2a). The volume fraction of the glial compartment and the hydrostatic pressure have also increased. The increased hydrostatic pressure in the stimulated region also raises the hydrostatic pressure in locations far away from the stimulated region. The increased pressure also drives the flow from stimulated region to the unstimulated region because the glial compartment is a connected space (Fig. 4.2d), a longitudinal syncytium. In the unstimulated region, the water flows out of the glial compartment into the unstimulated region because of the increased hydrostatic pressure in the glial compartment (Fig 4.2c). Then, because the fluid is incompressible, the fluid in the unstimulated region flows back to the stimulated region (Fig. 4.2b). The schematic graph of water circulation in the optic nerve is summarized in Fig. 4.3b. This is a summary of our results. It is not a compartment model. Our models are distributed.

In Fig. 4.2e&f, we show the volume change of extracellular space. In the stimulated

region, the extracellular space decreases because the water flows into the glial cell; while in the unstimulated region, the extracellular space swells because of water flow spatial buffering [93].

In sum, during a train of action potentials in the axon, the potassium flux transport pattern and potassium flux strength across the glia membrane and through the extracellular pathway are the same for both radial regions, inner and outer. The glial compartment pathway is the dominant clearance mechanism of the potassium accumulated in the extracellular stimulated region, in both cases.

### (b) After axon firing period

After the stimulus period, the main potassium clearance mechanism is the passive flow from extracellular space to glial compartment through the glial membrane. The potassium flux in extracellular region and glial compartment is negligible. In these calculations, the extracellular region and the glial compartment could be approximated as a single compartment. We show a schematic figure of potassium flux pattern in Fig. 4.6a. This is a summary and sketch of our results. We did not use a compartment model. Our model is distributed.

In the Fig. 4.4, we show the total potassium flux and cumulative potassium flux through  $M_S, E_T, M_{NS}$ , and  $G_T$  after axon firing period  $[T_{sti}, T_{af}]$ . For both cases, the strength of potassium fluxes through the glial transmembrane pathway ( $M_S$ ) and extracellular pathway have dramatically decreased after the axon stopped firing.

Fig. 4.4 e shows that in both cases (inner stimulus and outer stimulus), the potassium flows into the stimulated glial compartment after the axon firing period. Fig. 4.4g shows that the potassium flux through the glial membrane in the non-stimulated region reverses its direction for a short time after axon stop firing. This occurs because the extracellular potassium concentration becomes evenly distributed in both the stimulated and non-stimulated extracellular space.

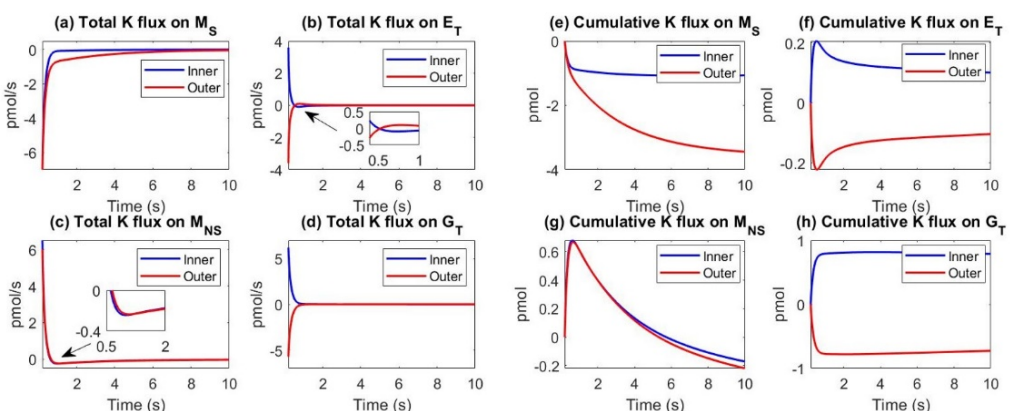


Figure 4.4 a-d: potassium flux through  $M_S, E_T, M_{NS}$ , and  $G_T$  after a train action potentials. The normal direction of potassium flux through glial transmembrane ( $M_S$  and  $M_{NS}$ ) points to extracellular

space; The normal direction of transition region in extracellular space ( $E_T$ ) ands glial compartment ( $G_T$ ) is radial direction. e-h: cumulative potassium flux after axon firing.

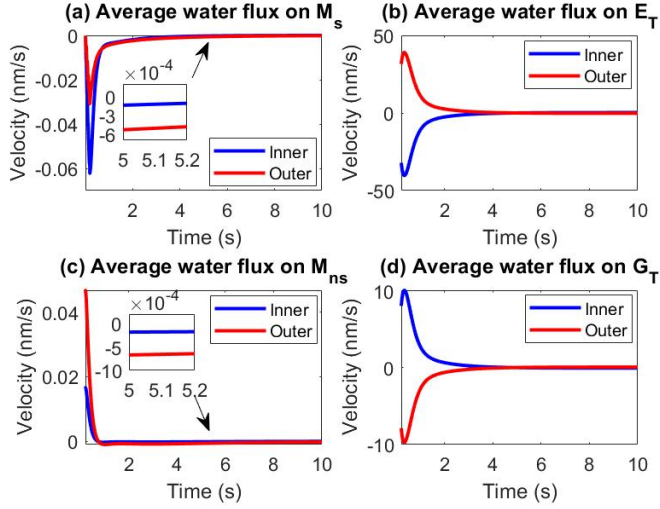


Figure 4.5 a-d: Average water velocity through  $M_s$ ,  $E_T$ ,  $M_{ns}$  and  $G_T$  after a train of axon firing.

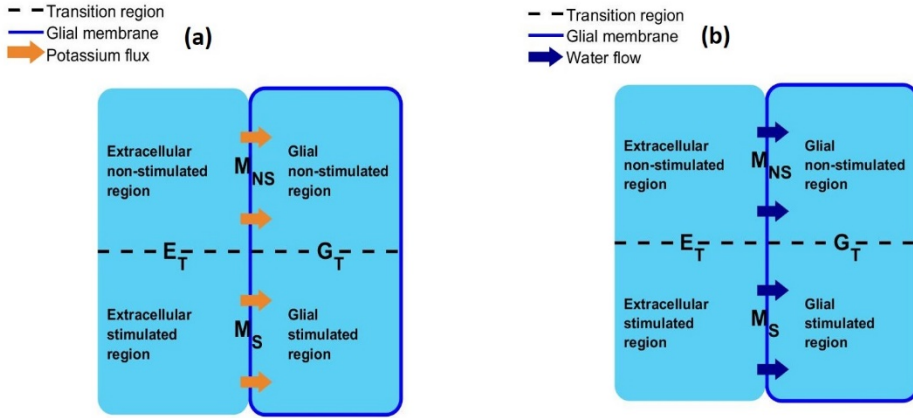


Figure 4.6 a: Schematic graph of the potassium flux after the axon was stimulated. The potassium flux leaks into the glial compartment from the extracellular space through the glial membrane in both stimulated and unstimulated regions. The potassium flux in the extracellular space and glial compartment is negligible. b: Schematic graph of the water flux after the axon was stimulated. Note these graphs are graphs that summarize outputs of large numbers of calculations solving partial differential equations in longitudinal and radial spatial directions and time. They do not represent a compartmental model. They are the output of a model distributed in space

In the Fig. 4.4f, in the extracellular space, potassium flows back to the stimulus region from the non-stimulus region via the extracellular pathway (in both cases). Accordingly, Fig. 4.5 shows that after the axon stops firing, the water flow inside the compartments becomes almost zero. The water flows through both stimulated and unstimulated glial membrane into the glial compartment, which is the same as the schematic graph Fig. 4.6b.

In sum, after the axon stops firing action potentials, the extracellular potassium concentration is quickly transported in the glial compartment and extracellular pathway. The main clearance of potassium is through the glia membrane in both stimulated and unstimulated regions. The potassium flux through the extracellular pathway becomes weaker after the axon stops firing action potentials.

Fig. 4.7a&b, we show the variation of the potassium concentration in the extracellular stimulated and unstimulated regions, respectively. The peak potassium concentration in the stimulated region is higher in the outer stimulated case compared to the inner stimulated case. As discussed previously, the strength of potassium clearance is the same for both cases, while in the outer radial stimulated case, there is three times as much potassium in the extracellular space during the axon firing as in the inner radial stimulated case.

The equality of potassium clearance in both cases also explains why the potassium concentration drops faster in the inner radial stimulated case than the outer one after axon stop firing. We provide a decay timetable in the appendix.

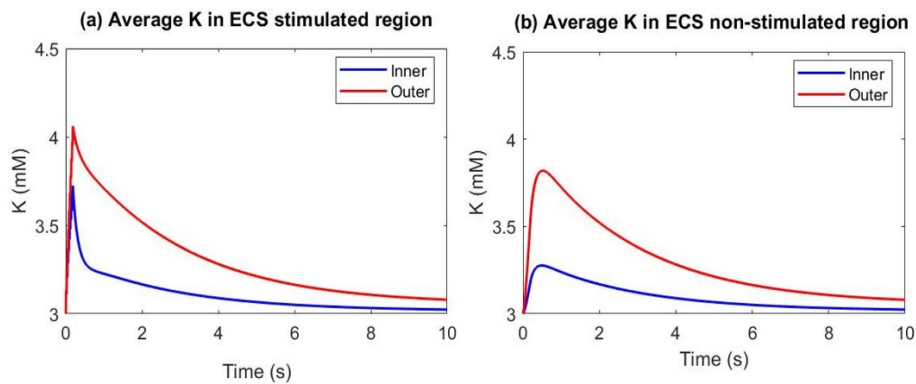


Figure 4.7 a-b: potassium concentration variation in the extracellular simulated region and non-stimulated region.

#### 4.1.2 Random distributed stimulated

In this section, we study whether random stimulation patterns in space differ from spatially uniform patterns. We apply a train of stimulus to four randomly distributed stimulated regions in the radial direction. The strength and duration of the stimulus is same as in the section 4 and the current is applied at the same longitudinal location ( $z = z_0$ ). The details of the radial stimulated location in each case has showed in the Fig. 4.8.

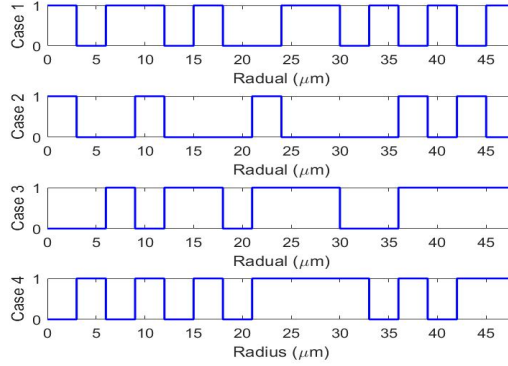


Figure 4.8: The stimulated radial segments in each case. The intervals with value 1 are stimulated segments and the intervals with value 0 are unstimulated segments.

### (a) During a train of axon firing

We compare the spatially random stimulated case (case 1, the rest cases are similar and shown in an appendix) with the inner radial region stimulated case in the Fig. 4.9a-d. During a train of axon firing, Fig. 4.9a&b, shows, in the randomly stimulated case, that the potassium clearance through the glial transmembrane ( $M_S$ ) has been reduced while the potassium flux through extracellular pathway in transition region ( $E_T$ ) has dramatically increased. Fig. 4.9e&f shows that the major clearance pathway in the randomly stimulated cases becomes the extracellular pathway in transition region ( $E_T$ ). More potassium flux goes through the extracellular path in the transition region in compare to it goes through glial membrane in the stimulated region. This differs from the outer and inner stimulated cases, where the glial transmembrane ( $M_S$ ) dominates as seen in Fig. 4.1e&f.

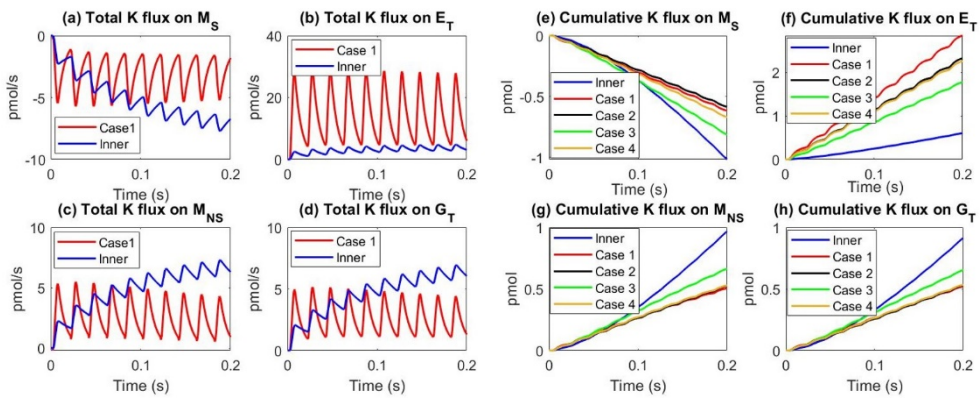


Figure 4.9 a-d: the comparison between the spatially random stimulated case with the spatially uniform radial (inner) case during a train of axon firing (the directional of the normal vector in the radial direction outward, from stimulated region to unstimulated region. The glial transmembrane flux normal direction points to the extracellular space). e-f: the cumulative flux comparison in  $M_S$ ,  $E_T$ ,  $M_{NS}$ , and  $G_T$  during a train of axon action potentials.

Fig. 4.9a-d shows that in inner stimulated case (blue line), the potassium flux strength

gradually increased with small oscillation in each axon stimulus time period; While in the spatially random stimulated case (red line), the potassium flux strength shows a periodic pattern in time with larger oscillation in each stimulus period. The reason for this quite different potassium flux pattern is that the extra potassium in the extracellular stimulated region has been cleared quicker in the random select case. So, in each stimulus period, the potassium flux decreases dramatically since the potassium goes back to its resting state. While in the inner stimulus case, for each stimulus period, the clearance of potassium is slower and there is accumulation potassium in the stimulated extracellular space.

In sum, Fig. 4.9e&f, during a train of axon firing, much more potassium flux goes through the extracellular pathway through transition region ( $E_T$ ), which reduces the effect of glial compartment pathway in the stimulated region ( $M_S$ ).

### (b) After axon firing period

After the axon stops firing action potentials, both the spatially random case and the uniform inner case have similar reduced potassium fluxes, See  $M_S$ ,  $E_T$ ,  $M_{NS}$ , and  $G_T$ . In Fig. 4.10e&g shows that the main pathway for potassium clearance (after the action potentials cease) is through the glial transmembrane pathway.

Fig. 4.10h shows a large difference between the spatially random and the spatially uniform case in some properties. The cumulative transport of potassium flux through the glial compartment transition region in the spatially random cases is much smaller than it is in the uniform inner case. This is because during axon firing period, the extracellular potassium in the stimulated region has been quickly removed in the random cases. The potassium concentration became more homogeneous and there was less difference between the stimulated region and non-stimulated regions. As a result, the glial compartment electric potential  $\phi_{gl}$  becomes homogeneous in entire glial compartment and the electric drift flow in the glial transition region was reduced for potassium.

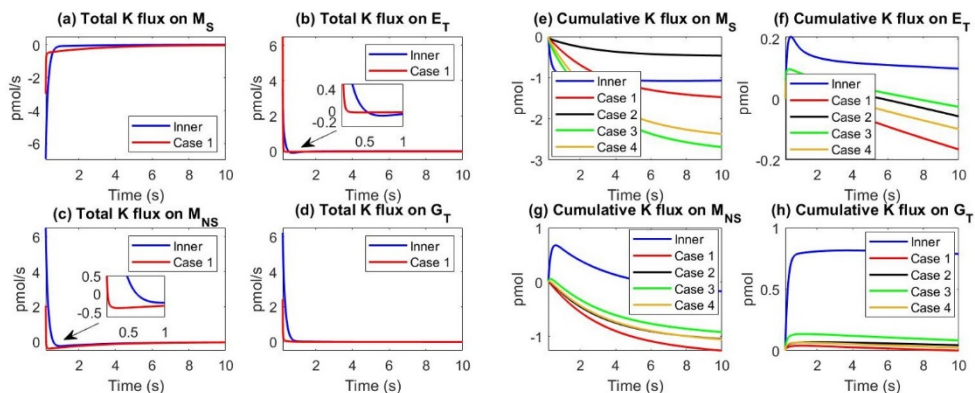


Figure 4.10: a-d: the comparison between the spatially random case with the uniform inner radial case after a train of action potentials Vector directions as defined previously. e-f: the cumulative flux comparison in  $M_S$ ,  $E_T$ ,  $M_{NS}$ , and  $G_T$  after a train of action potentials.

### (c) Potassium clearance and fluid velocity in the extracellular space and glia compartment

Since the potassium goes less through the glial transmembrane pathway in the stimulated region, the osmosis in the extracellular  $k_B T O_{ex}$  and in glial  $k_B T O_{gl}$ , and variation in the stimulated region has been reduced. Therefore, the strength of the velocities decreases in both glia and extracellular compartment since the decrease of the glial transmembrane water flow as show in Fig. 4.11c&d. The average potassium concentration changes in both stimulated region and non-stimulated region is shown in the Fig. 4.11a&b and its decay time in each case is in the appendix.

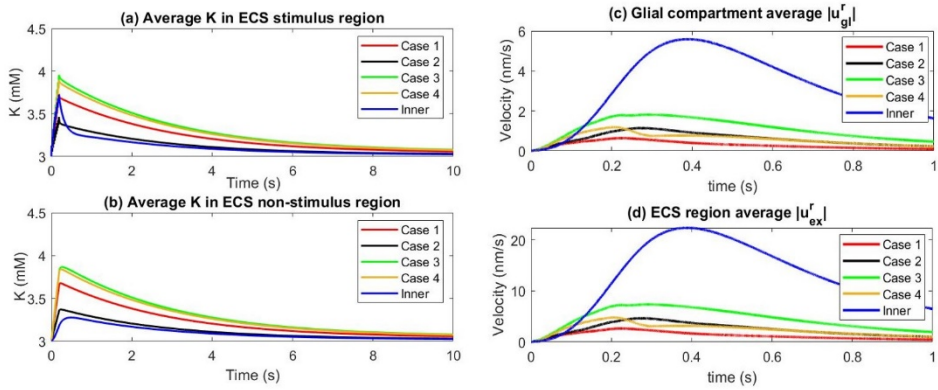


Figure 4.11: a-b: variation of potassium concentration in the extracellular simulated region and unstimulated regions. c-d: average glial compartment radial absolute velocity and extracellular space radial absolute velocity.

## 4.2 Effect of NKCC and non-selective pathway on pia mater

In this section, we consider the effect of glial membrane conductance and a non-selective pathway on the pia boundary on the potassium clearance process. We first introduce the NKCC channel into the glial membrane, as widely studied in the literature. We compare simulation results between the model with NKCC and without NKCC. In the second part, we consider the effect of a non-selective pathway in the pia mater boundary. That pathway allows the convection flux through an extracellular pathway out of the optic nerve. We investigate how these factors affect the potassium clearance.

### 4.2.1 Effect of NKCC on the glial membrane

We introduce a model of NKCC channels in the glial membrane as in the [70, 94], We describe the  $K^+$ ,  $Na^+$  and  $Cl^-$  flux through the NKCC channel in the glial membrane as in [70, 94]

$$J_{NKCC}^K = -\frac{I_{max}^{NKCC}}{e z^K} \log \left( \frac{c_{ex}^K c_{ex}^{Na}}{c_{gl}^K c_{gl}^{Na}} \left( \frac{c_{ex}^{Cl}}{c_{gl}^{Cl}} \right)^2 \right),$$

$$J_{NKCC}^{Na} = -\frac{I_{max}^{NKCC}}{ez^{Na}} \log \left( \frac{C_{ex}^K C_{ex}^{Na}}{C_{gl}^K C_{gl}^{Na}} \left( \frac{C_{ex}^{Cl}}{C_{gl}^{Cl}} \right)^2 \right),$$

$$J_{NKCC}^{Cl} = 2 \frac{I_{max}^{NKCC}}{ez^{Cl}} \log \left( \frac{C_{ex}^K C_{ex}^{Na}}{C_{gl}^K C_{gl}^{Na}} \left( \frac{C_{ex}^{Cl}}{C_{gl}^{Cl}} \right)^2 \right).$$

To compare the effect of NKCC without NKCC, we keep the potassium and sodium concentration as well as the resting electric potential in the glial compartment and extracellular space the same. In the resting state, we set sodium and potassium current through NKCC channel to be comparable with respect to the Na/K pump current as in the paper[70, 95]. In the appendix, we provide the two sets of parameters (NKCCa and NKCCb) that balance the additional NKCC current through the glial membrane.

In the simulation below, we compare the models with and without NKCC. The stimulated region Fig. 4.12, shows the cumulative potassium flux through the  $M_S, E_T, M_{NS}$ , and  $G_T$  during and after stimuli.

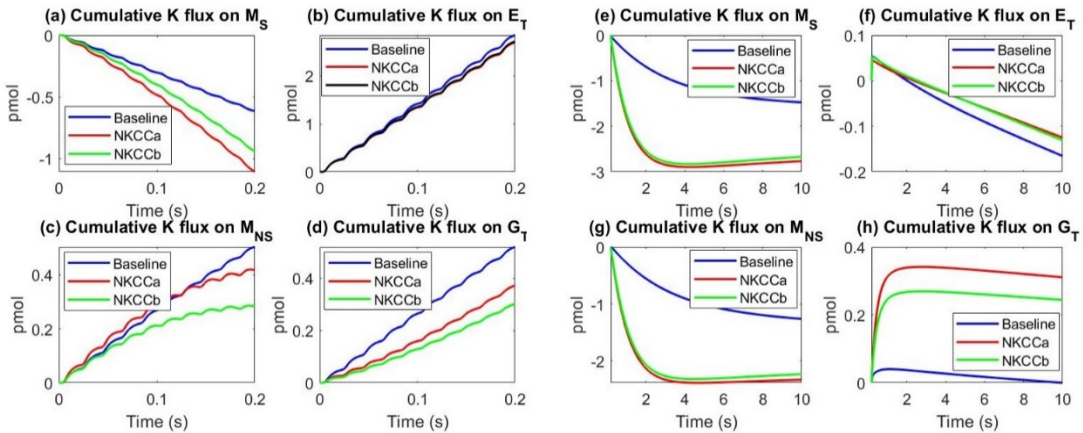


Figure 4.12: a-d: the cumulative flux comparison in  $M_S, E_T, M_{NS}$ , and  $G_T$  during a train of action potentials. e-h: the cumulative flux comparison in  $M_S, E_T, M_{NS}$ , and  $G_T$  after a train of action potentials.

Fig. 4.12a shows that more potassium goes through the glial membrane in the simulated region during axon firing when NKCC is present, which is hardly surprising. The NKCC channel has enhanced the transport of potassium through the glial membrane after the axon stopped firing as in Fig. 4.12e&g.

Fig. 4.13a&b shows the variation of potassium concentration in the extracellular space in the stimulated and unstimulated cases. The potassium decay in much faster when NKCC is present presumably because NKCC allows larger movement of potassium into the glial compartment. We provide the decay timetable in the appendix.

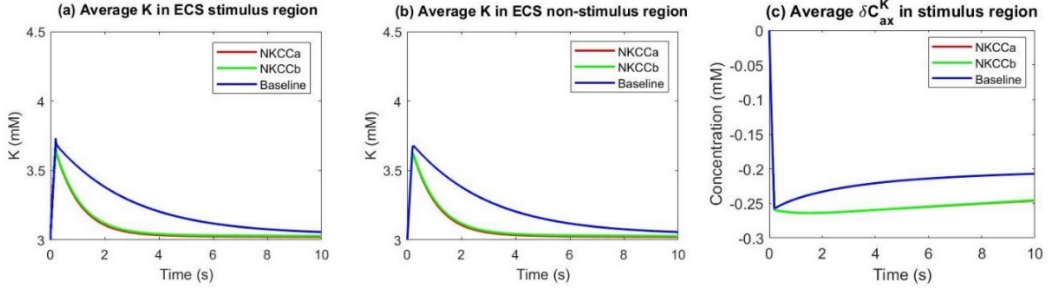


Figure 4.13: a-b: extracellular potassium concentration variation comparison between the model with NKCC and baseline model (without NKCC). c: average potassium variation in the axon stimulated region.

The quicker potassium is taken into glial compartment by the NKCC, the slower the return of potassium concentration back to resting state. Fig. 4.13c, shows the variation of the potassium concentration in the stimulated region. After action potentials cease, the potassium movement back to the axon compartment is reduced in the model with NKCC channel. Fig. 4.13c, shows that the average potassium concentration in the baseline model increases faster after the axon stops firing than in the model with NKCC.

#### 4.2.2 Non-selective pathway through the pia matter

In this section, we consider the effect of a non-selective pathway across the pia boundary. The nonselective pathway allows both ion and water fluid transport through the cleft between the cells in the pia mater. We assume that the water fluid goes through the non-selective pathway only depends on the hydrostatic pressure difference. Therefore, the fluid condition on pia boundary ( $\Gamma_7$ ) in (2.27) become

$$\mathbf{u}_{ex}^{OP} \cdot \hat{\mathbf{r}} = \mathbf{u}_{ex}^{SAS} \cdot \hat{\mathbf{r}} = u_{pia}^m + u_{pia}^{ns}, \quad \text{on } \Gamma_7$$

where

$$u_{pia}^m = L_{pia}^m \left( P_{ex}^{OP} - P_{ex}^{SAS} - \gamma_{pia} k_B T (O_{ex}^{OP} - O_{ex}^{SAS}) \right), \quad u_{pia}^{ns} = L_{pia}^{ns} (P_{ex}^{OP} - P_{ex}^{SAS}).$$

The non-selective pathway between the cell clefts provides an additional pathway for diffusion, electric drift as well as convection for ions. We modify the boundary condition (2.41) for ion on pia boundary ( $\Gamma_7$ ) as

$$\mathbf{J}_{ex}^{i,OP} \cdot \hat{\mathbf{r}} = \mathbf{J}_{ex}^{i,SAS} \cdot \hat{\mathbf{r}} = \frac{G_{pia}^i + G^{ns}}{z^i e} (\phi_{ex}^{OP} - \phi_{ex}^{SAS} - E_{pia}^i) + C_{ex}^i u_{pia}^{ns}, \quad i = \text{Na}^+, \text{K}^+, \text{on } \Gamma_7$$

Here  $G^{ns}$  is the additional conductance due to the non-selective pathway and  $C_{ex}^i u_{pia}^{ns}$  is the convection flux through the non-selective pathway on pia boundary.

In the simulation below, we compare the model with non-selective pathway with the model without the non-selective pathway. We choose the comparison parameter to

be

$$\frac{G^{ns}}{G^K_{pia}} = \frac{L_{pia}^{ns}}{L_{pia}^m} = 10.$$

In the Fig. 4.14, we show the potassium variation in extracellular space and the cumulative potassium flux through the pia mater and glial membrane.

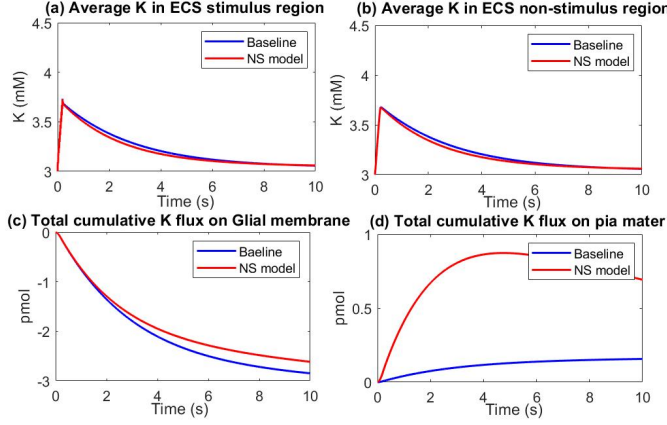


Figure 4.14: a-b: extracellular potassium concentration variation comparison between the model with non-selective pathway on pia boundary and baseline model (without non-selective pathway).c: total cumulative potassium flux through glial membrane. d: total cumulative potassium flux though pia boundary.

The amount of potassium leak out of the optic nerve through the pia boundary is dramatically increased when the pathway is present in Fig. 4.14d. However, the dominant pathway of potassium clearance is still through the glial membrane as previously in Fig. 4.14c. This is because the total glial membrane area is much larger than the surface area on pia boundary,

$$\frac{2\pi R_a L}{V_{on} \mathcal{M}_{gl}} = O(10^{-3}),$$

where the  $V_{on}$  is the total optic nerve volume and  $\mathcal{M}_{gl}$  is the glial membrane per unit volume. Fig. 4.14a&b shows that with the non-selective pathway on the pia boundary does not accelerate the potassium clearance rate very much.

## 5. Conclusion

In this work, we propose a tridomain model to study potassium clearance in the optic nerve of *Necturus* in a series of experiments from Richard Orkand and the Harvard group [7, 8]. Our model, analysis, and simulations provide a detailed picture of the role of glial cells in buffering the concentration of ions, mostly in the narrow extracellular space. While the nerve axons are being stimulated, both the extracellular space and glial cells play important roles. They both clear extra potassium from the narrow extracellular space while the axon is firing action potentials. After the action

potentials stop, the potassium remaining in the extracellular space is cleared by the glial compartment.

Our model shows that the longitudinal *electrical syncytium* of the glial cells is critical for clearing potassium (from the extracellular space) when the neuron fires. The inward glial transmembrane potassium flux in the stimulated region is almost the same as the outward potassium flux out to the extracellular space in the non-stimulated region, in response to the change in potassium concentration between the extracellular space in the stimulated and unstimulated regions. This is because the electric potential spreads through the connected cells in the glial compartment. The glial electric potential in the unstimulated region becomes more positive in response to the depolarization of the glial electric potential in the stimulus region. The ‘cable properties’ of the glial compartment are a feature that separates our field model with its partial differential equations from the compartment models in the literature that use ordinary differential equations. Compartment models lack the combination of space and time dependence needed to describe the temporal and spatial spread of potential. The combined temporal and spatial spread of potential is a crucial property of neurons. Here we show that the combined temporal and spatial spread of potential is a crucial property of the glia, and the narrow extracellular space between glia and neurons. In a sense, we extend the electrical cable theory of neurons to a cable theory for flow in neuron, glia, and the narrow extracellular space between them.

We discuss the effect of enhanced potassium conductance in the glial membrane and nerve membranes of the pia mater. On the one hand, incorporating NKCC channels into the glial membrane increases potassium clearance. Potassium clearance time is much shorter than that predicted by the baseline model (without NKCC channels in the glial membrane). On the other hand, an additional non-selective pathway in another location—in the pia mater—does not have significant effect on potassium clearance. This is not surprising since the total membrane area of the glial membrane in the optic nerve is much greater than the effective surface membrane of nerves in the pia mater.

Finally, our distributed model and its partial differential equations can be generalized to describe ionic and water transport in tissues with more complicated and heterogeneous structures and with glymphatic pathways connected to the circulatory system. We expect that the spatially nonuniform distribution of ion and water channels and transporters will be used in many structures in the central nervous system to control flow.

## References

1. Hodgkin, A.L., A.F. Huxley, and B. Katz, *Measurement of current- voltage relations in the membrane of the giant axon of Loligo*. J. Physiol. (London), 1952. **116**: p. 424-448.
2. Hodgkin, A., A. Huxley, and B. Katz, *Ionic Currents underlying activity in the giant axon of the squid*. Arch. Sci. physiol., 1949. **3**: p. 129-150.
3. Hodgkin, A.L. and A.F. Huxley, *Currents carried by sodium and potassium ions through the membrane of the giant axon of Loligo*. J. Physiol., 1952. **116**: p. 449-472.
4. Frankenhaeuser, B. and A.L. Hodgkin, *The after-effects of impulses in the giant nerve fibres of Loligo*. Journal of Physiology (London), 1956. **131**: p. 341-376.
5. Hodgkin, A.L. and A.F. Huxley, *A quantitative description of membrane current and its application to conduction and excitation in nerve*. J. Physiol., 1952. **117**: p. 500-544.
6. Kuffler, S.W. and J.G. Nicholls, *The physiology of neuroglial cells*, in *Ergebnisse der physiologie biologischen chemie und experimentellen pharmakologie*. 1966, Springer. p. 1-90.
7. Kuffler, S.W., J.G. Nicholls, and R.K. Orkand, *Physiological properties of glial cells in the central nervous system of amphibia*. J Neurophysiol, 1966. **29**(4): p. 768-87.
8. Orkand, R.K., J.G. Nicholls, and S.W. Kuffler, *Effect of nerve impulses on the membrane potential of glial cells in the central nervous system of amphibia*. J Neurophysiol, 1966. **29**(4): p. 788-806.
9. Nedergaard, M. and S.A. Goldman, *Glymphatic failure as a final common pathway to dementia*. Science, 2020. **370**(6512): p. 50.
10. O'Connell, R. and Y. Mori, *Effects of Glia in a Triphasic Continuum Model of Cortical Spreading Depression*. Bull Math Biol, 2016. **78**(10): p. 1943-1967.
11. Tuttle, A., J. Riera Diaz, and Y. Mori, *A computational study on the role of glutamate and NMDA receptors on cortical spreading depression using a multidomain electrodiffusion model*. PLoS Comput Biol, 2019. **15**(12): p. e1007455.
12. Ayata, C. and M. Lauritzen, *Spreading Depression, Spreading Depolarizations, and the Cerebral Vasculature*. Physiological Reviews, 2015. **95**(3): p. 953.
13. Wei, Y., G. Ullah, and S.J. Schiff, *Unification of Neuronal Spikes, Seizures, and Spreading Depression*. The Journal of Neuroscience, 2014. **34**(35): p. 11733-11743.
14. Ullah, G., et al., *The Role of Cell Volume in the Dynamics of Seizure, Spreading*

*Depression, and Anoxic Depolarization.* PLoS Comput Biol, 2015. **11**(8): p. e1004414.

- 15. Ayata, C. and M. Lauritzen, *Spreading depression, spreading depolarizations, and the cerebral vasculature.* Physiological reviews, 2015. **95**(3): p. 953-993.
- 16. Mori, Y., *A multidomain model for ionic electrodiffusion and osmosis with an application to cortical spreading depression.* Physica D: Nonlinear Phenomena, 2015. **308**(15): p. 94-108.
- 17. Miura, R.M., H. Huang, and J.J. Wylie, *Cortical spreading depression: An enigma.* The European Physical Journal, 2007. **147**: p. 287-302.
- 18. Gakuba, C., et al., *General anesthesia inhibits the activity of the "glymphatic system".* Theranostics, 2018. **8**(3): p. 710.
- 19. Jiang, Q., et al., *Impairment of the glymphatic system after diabetes.* Journal of Cerebral Blood Flow & Metabolism, 2017. **37**(4): p. 1326-1337.
- 20. Abbott, N.J., et al., *The role of brain barriers in fluid movement in the CNS: is there a 'glymphatic' system?* Acta neuropathologica, 2018. **135**(3): p. 387-407.
- 21. Jessen, N.A., et al., *The glymphatic system: a beginner's guide.* Neurochemical research, 2015. **40**(12): p. 2583-2599.
- 22. Mestre, H., Y. Mori, and M. Nedergaard, *The Brain's Glymphatic System: Current Controversies.* Trends in Neurosciences, 2020. **43**(7): p. 458-466.
- 23. Xu, S., et al., *Osmosis through a Semi-permeable Membrane: a Consistent Approach to Interactions.* arXiv preprint arXiv:1806.00646, 2018.
- 24. Mori, Y., C. Liu, and R.S. Eisenberg, *A model of electrodiffusion and osmotic water flow and its energetic structure.* Physica D: Nonlinear Phenomena, 2011. **240**(22): p. 1835-1852.
- 25. Eisenberg, B., Y. Hyon, and C. Liu, *Energy Variational Analysis EnVarA of Ions in Water and Channels: Field Theory for Primitive Models of Complex Ionic Fluids.* Journal of Chemical Physics, 2010. **133**(10): p. 104104.
- 26. Donaldson, P.J., *Fluid in equals fluid out--evidence for circulating fluid fluxes in the lens.* Invest Ophthalmol Vis Sci, 2012. **53**(12).
- 27. Donaldson, P.J., et al., *The physiological optics of the lens.* Prog Retin Eye Res, 2017. **56**: p. e1-e24.
- 28. Donaldson, P.J., L.S. Musil, and R.T. Mathias, *Point: A critical appraisal of the lens circulation model--an experimental paradigm for understanding the maintenance of lens transparency?* Invest Ophthalmol Vis Sci, 2010. **51**(5): p. 2303-6.
- 29. Mathias, R.T., J. Kistler, and P. Donaldson, *The lens circulation.* J Membr Biol, 2007. **216**(1): p. 1-16.
- 30. Mathias, R.T., J.L. Rae, and G.J. Baldo, *Physiological properties of the normal lens.* Physiol Rev, 1997. **77**(1): p. 21-50.
- 31. Mathias, R.T., et al., *The localization of transport properties in the frog lens.* Biophys J, 1985. **48**(3): p. 423-34.
- 32. Baldo, G.J. and R.T. Mathias, *Spatial variations in membrane properties in the intact rat lens.* Biophys J, 1992. **63**(2): p. 518-29.
- 33. Eisenberg, R.S. and J.L. Rae, *Current-voltage relationships in the crystalline*

*lens. J Physiol*, 1976. **262**(2): p. 285-300.

34. Barsoukov, E. and J.R. Macdonald, *Impedance spectroscopy: theory, experiment, and applications*. 2018: John Wiley & Sons.

35. Mathias, R.T., J.L. Rae, and R.S. Eisenberg, *The lens as a nonuniform spherical syncytium*. *Biophys J*, 1981. **34**(1): p. 61-83.

36. Gao, J., et al., *Feedback Regulation of Intracellular Hydrostatic Pressure in Surface Cells of the Lens*. *Biophys J*, 2015. **109**(9): p. 1830-9.

37. Gao, J., et al., *The effect of size and species on lens intracellular hydrostatic pressure*. *Invest Ophthalmol Vis Sci*, 2013. **54**(1): p. 183-92.

38. Gao, J., et al., *Lens intracellular hydrostatic pressure is generated by the circulation of sodium and modulated by gap junction coupling*. *J Gen Physiol*, 2011. **137**(6): p. 507-20.

39. Gao, J., et al., *Disruption of the lens circulation causes calcium accumulation and precipitates in connexin mutant mice*. *Am J Physiol Cell Physiol*, 2018. **314**(4): p. C492-C503.

40. Kumari, S., et al., *Aquaporin 0 Modulates Lens Gap Junctions in the Presence of Lens-Specific Beaded Filament Proteins*. *Invest Ophthalmol Vis Sci*, 2017. **58**(14): p. 6006-6019.

41. Hall, J.E. and R.T. Mathias, *The aquaporin zero puzzle*. *Biophys J*, 2014. **107**(1): p. 10-5.

42. Mathias, R.T., T.W. White, and X. Gong, *Lens gap junctions in growth, differentiation, and homeostasis*. *Physiol Rev*, 2010. **90**(1): p. 179-206.

43. Ayata, C. and M. Lauritzen, *Spreading Depression, Spreading Depolarizations, and the Cerebral Vasculature*. Vol. 95. 2015. 953-993.

44. Mathias, R.T. and H. Wang, *Local osmosis and isotonic transport*. *J Membr Biol*, 2005. **208**(1): p. 39-53.

45. McLaughlin, S. and R.T. Mathias, *Electro-osmosis and the reabsorption of fluid in renal proximal tubules*. *J Gen Physiol*, 1985. **85**(5): p. 699-728.

46. Diamond, J.M. and W.H. Bossert, *Standing-gradient osmotic flow: A mechanism for coupling of water and solute transport in epithelia*. *The Journal of general physiology*, 1967. **50**(8): p. 2061-2083.

47. Patlak, C., D. Goldstein, and J. Hoffman, *The flow of solute and solvent across a two-membrane system*. *Journal of Theoretical Biology*, 1963. **5**(3): p. 426-442.

48. Loo, D.D., E.M. Wright, and T. Zeuthen, *Water pumps*. *The Journal of physiology*, 2002. **542**(1): p. 53-60.

49. Desjeux, J.-F., et al., *Effect of cholera toxin in Na transport in intestine*. *Pediatric Research*, 1974. **8**(4): p. 380-380.

50. Curran, P.F. and J.R. Macintosh, *A model system for biological water transport*. *Nature*, 1962. **193**: p. 347-348.

51. Zhu, Y., et al., *A Bidomain Model for Lens Microcirculation*. *Biophysical Journal*, 2019. **116**(6): p. 1171-1184 Preprint available at <https://arxiv.org/abs/1810.04162>.

52. Malcolm, D.T.K., *A computational model of the ocular lens*. 2006,

ResearchSpace@ Auckland.

- 53. Einighammer, J., et al., *The individual virtual eye: a computer model for advanced intraocular lens calculation*. Journal of optometry, 2009. **2**(2): p. 70-82.
- 54. Vaghefi, E., N. Liu, and P.J. Donaldson, *A computer model of lens structure and function predicts experimental changes to steady state properties and circulating currents*. Biomed Eng Online, 2013. **12**: p. 85.
- 55. Vaghefi, E., et al., *Development of a 3D finite element model of lens microcirculation*. Biomed Eng Online, 2012. **11**: p. 69.
- 56. Norman, R.E., et al., *Finite element modeling of the human sclera: influence on optic nerve head biomechanics and connections with glaucoma*. Experimental eye research, 2011. **93**(1): p. 4-12.
- 57. Ethier, C., et al., *Finite Element Modeling of the Human Sclera: Influence on ONH Biomechanics and Connections With Glaucoma*. Investigative Ophthalmology & Visual Science, 2009. **50**(13): p. 4889-4889.
- 58. Gardiner, B.S., et al., *Computational modeling of fluid flow and intra-ocular pressure following glaucoma surgery*. PLoS One, 2010. **5**(10): p. e13178.
- 59. Eisenberg, B., *Validating the need to validate code*. Physics Today, 2005. **58**: p. p.13 (Letter to the Editor).
- 60. Post, D.E. and L.G. Votta, *Computational Science Demands a New Paradigm*. Physics Today, 2005. **58**: p. 35-41.
- 61. Maginn, E.J., *From discovery to data: What must happen for molecular simulation to become a mainstream chemical engineering tool*. AIChE Journal, 2009. **55**(6): p. 1304-1310.
- 62. Acton, F.S., *Real Computing Made Real: Preventing Errors in Scientific and Engineering Calculations*. 2013: Dover Publications.
- 63. Tuckwell, H.C. and R.M. Miura, *A mathematical model for spreading cortical depression*. Biophysical Journal, 1978. **23**(2): p. 257-276.
- 64. Postnov, D.E., L.S. Ryazanova, and O.V. Sosnovtseva, *Functional modeling of neural-glial interaction*. BioSystems, 2007. **89**(1-3): p. 84-91.
- 65. Chang, J.C., et al., *A mathematical model of the metabolic and perfusion effects on cortical spreading depression*. PLoS One, 2013. **8**(8): p. e70469.
- 66. Yao, W., H. Huang, and R.M. Miura, *A continuum neuronal model for the instigation and propagation of cortical spreading depression*. Bulletin of mathematical biology, 2011. **73**(11): p. 2773-2790.
- 67. Bellinger, S., G. Miyazawa, and P. Steinmetz, *Submyelin potassium accumulation may functionally block subsets of local axons during deep brain stimulation: a modeling study*. Journal of neural engineering, 2008. **5**(3): p. 263.
- 68. Chen, K.C. and C. Nicholson, *Spatial buffering of potassium ions in brain extracellular space*. Biophysical journal, 2000. **78**(6): p. 2776-2797.
- 69. Reichenbach, A., et al., *What do retinal Müller (glial) cells do for their neuronal 'small siblings'*? Journal of chemical neuroanatomy, 1993. **6**(4): p. 201-213.

70. Østby, I., et al., *Astrocytic mechanisms explaining neural-activity-induced shrinkage of extraneuronal space*. PLoS computational biology, 2009. **5**(1): p. e1000272.

71. Sibille, J., et al., *The neuroglial potassium cycle during neurotransmission: role of Kir4. 1 channels*. PLoS computational biology, 2015. **11**(3): p. e1004137.

72. Bellot-Saez, A., et al., *Astrocytic modulation of neuronal excitability through K<sup>+</sup> spatial buffering*. Neuroscience & Biobehavioral Reviews, 2017. **77**: p. 87-97.

73. Nicholson, C. and S. Hrabětová, *Brain Extracellular Space: The Final Frontier of Neuroscience*. Biophysical Journal, 2017. **113**(10): p. 2133-2142.

74. Hou, R., et al., *Intracranial pressure (ICP) and optic nerve subarachnoid space pressure (ONSP) correlation in the optic nerve chamber: the Beijing Intracranial and Intraocular Pressure (iCOP) study*. brain research, 2016. **1635**: p. 201-208.

75. Morgan, W.H., et al., *Cerebrospinal fluid pressure and the eye*. British Journal of Ophthalmology, 2016. **100**(1): p. 71-77.

76. Killer, H., et al., *Cerebrospinal fluid dynamics between the intracranial and the subarachnoid space of the optic nerve. Is it always bidirectional?* Brain, 2007. **130**(2): p. 514-520.

77. Band, L.R., et al., *Intracellular flow in optic nerve axons: a mechanism for cell death in glaucoma*. Investigative ophthalmology & visual science, 2009. **50**(8): p. 3750-3758.

78. Nicholson, C., *Diffusion and related transport mechanisms in brain tissue*. Reports on progress in Physics, 2001. **64**(7): p. 815.

79. Filippidis, A.S., et al., *Permeability of the arachnoid and pia mater. The role of ion channels in the leptomeningeal physiology*. Child's Nervous System, 2012. **28**(4): p. 533-540.

80. Eisenberg, B., *Asking biological questions of physical systems: The device approach to emergent properties*. Journal of Molecular Liquids, 2018. **270**: p. 212-217. Preprint available on arXiv as <https://arxiv.org/abs/1801.05452>.

81. Hayreh, S.S., *The sheath of the optic nerve*. Ophthalmologica, 1984. **189**(1-2): p. 54-63.

82. Hayreh, S.S., *Ischemic optic neuropathy*. Progress in retinal and eye research, 2009. **28**(1): p. 34-62.

83. Jonas, J.B., E. Berenshtein, and L. Holbach, *Anatomic relationship between lamina cribrosa, intraocular space, and cerebrospinal fluid space*. Investigative ophthalmology & visual science, 2003. **44**(12): p. 5189-5195.

84. Feher, J.J., *Quantitative human physiology: an introduction*. 2017: Academic press.

85. Pérez-Pinzón, M., L. Tao, and C. Nicholson, *Extracellular potassium, volume fraction, and tortuosity in rat hippocampal CA1, CA3, and cortical slices during ischemia*. Journal of Neurophysiology, 1995. **74**(2): p. 565-573.

86. Wan, L., et al., *Self-Consistent Approach to Global Charge Neutrality in Electrokinetics: A Surface Potential Trap Model*. Physical Review X, 2014. **4**(1):

p. 011042.

- 87. Gardiner, B.S., et al., *Computational modeling of fluid flow and intra-ocular pressure following glaucoma surgery*. PloS one, 2010. **5**(10).
- 88. Pache, M. and P. Meyer, *Morphological changes of the retrobulbar optic nerve and its meningeal sheaths in glaucoma*. Ophthalmologica, 2006. **220**(6): p. 393-396.
- 89. Sigal, I.A., J.G. Flanagan, and C.R. Ethier, *Factors influencing optic nerve head biomechanics*. Investigative ophthalmology & visual science, 2005. **46**(11): p. 4189-4199.
- 90. Fitzhugh, R., *Thresholds and plateaus in the Hodgkin-Huxley nerve equations*. The Journal of general physiology, 1960. **43**(5): p. 867-896.
- 91. Song, Z., X. Cao, and H. Huang, *Electroneutral models for dynamic Poisson-Nernst-Planck systems*. Physical Review E, 2018. **97**(1): p. 012411.
- 92. Gao, J., et al., *Isoform-specific function and distribution of Na/K pumps in the frog lens epithelium*. J Membr Biol, 2000. **178**(2): p. 89-101.
- 93. Kofuji, P. and E.A. Newman, *Potassium buffering in the central nervous system*. Neuroscience, 2004. **129**(4): p. 1043-1054.
- 94. Lauf, P.K. and N.C. Adragna, *K-Cl cotransport: properties and molecular mechanism*. Cellular Physiology and Biochemistry, 2000. **10**(5-6): p. 341-354.
- 95. Murakami, S. and Y. Kurachi, *Mechanisms of astrocytic K<sup>+</sup> clearance and swelling under high extracellular K<sup>+</sup> concentrations*. The Journal of Physiological Sciences, 2016. **66**(2): p. 127-142.